

All-optical quantum computing using cubic phase gates

Niklas Budinger,^{1,*} Akira Furusawa,^{2,3} and Peter van Loock^{1,†}

¹*Johannes-Gutenberg University of Mainz, Institute of Physics, Staudingerweg 7, 55128 Mainz, Germany*

²*Department of Applied Physics, School of Engineering,*

The University of Tokyo, 7-3-1 Hongo, Bunkyo-ku, Tokyo 113-8656, Japan

³*Optical Quantum Computing Research Team, RIKEN Center for Quantum Computing, 2-1 Hirosawa, Wako, Saitama 351-0198, Japan*

If suitable quantum optical interactions were available, transforming the field mode operators in a nonlinear fashion, the all-photonics platform could be one of the strongest contenders for realizing a quantum computer. While single-photon qubits may be processed directly, “brighter” logical qubits may be embedded in individual oscillator modes, using so-called bosonic codes, for an in-principle fault-tolerant processing. In this paper, we show how elements of all-optical, universal, and fault-tolerant quantum computation can be implemented using only beam splitters together with single-mode cubic phase gates in reasonable numbers, and possibly off-line squeezed-state or single-photon resources. Our approach is based on a decomposition technique combining exact gate decompositions and approximate Trotterization. This allows for efficient decompositions of certain nonlinear continuous-variable multimode gates into the elementary gates, where the few cubic gates needed may even be weak or all identical, thus facilitating potential experiments. The final gate operations include two-mode controlled phase rotation and three-mode Rabi-type Hamiltonian gates, which are shown to be employable for realizing high-fidelity single-photon two-qubit entangling gates or creating high-quality Gottesman-Kitaev-Preskill states. We expect our method to be of general use with various applications, including those that rely on quartic Kerr-type interactions.

I. INTRODUCTION

The photonics platform offers some clear advantages to quantum computing in terms of scalability and general error robustness, depending on the encoding of the quantum information. In particular, unlike other, matter-based, solid-state or atomic platforms, photonic qubits can be operated at room temperature and high clock rates – as high as GHz or, in principle, even THz. In addition, recent optical continuous-variable time-domain approaches are extremely well scalable [1, 2].

However, there are also two main complications for the universal processing of photonic qubits or, more generally, quantum optical field modes: the presence of photon loss and the lack of sufficiently strong interactions that transform the mode operators in a nonlinear fashion. In many proposals, the lack of suitable optical nonlinearities on the level of the mode operator Hamiltonians is circumvented by introducing measurement-induced nonlinearities, possibly supplemented by an appropriately chosen nonclassical optical ancilla state [3–5]. A similar, but particularly efficient approach avoiding large coupling losses is one that, although still relying upon a nonclassical ancilla state, shifts part of the nonlinearity into the classical feedforward operations [6–8]. Nonetheless, on the level of the Hamiltonian of the field modes interacting with a nonlinear medium, weak cubic mode interactions do occur, and it has been known for long that, in principle, so-called cubic single-mode gates in combination with two-mode beam splitters as well as single-mode quadratic ro-

tations and linear shifts in phase space lead to a notion of universal continuous-variable (CV) multimode quantum information processing [9–12].

Still one problem remains that these naturally occurring cubic nonlinearities, such as three-wave mixing [13], generalized “trisqueezing” [14, 15], or certain cubic two-mode Hamiltonians [16], are not easy to exploit experimentally in a loss-tolerant and efficient way, exhibiting a sufficiently strong effective nonlinearity [17]. Another problem is that, even when assuming that robust, elementary cubic gates are experimentally available, the existing schemes require unrealistically many such cubic gates of sufficient and variable interaction strength, which even in a well-scalable time-domain approach would become impractical taking into account experimental errors and loss per physical gate. Here we address this latter problem and, assuming that cubic single-mode gates will be experimentally available [8], we propose gate decomposition techniques that lead to gate sequences of cubic single-mode gates and beam splitters of the order of ten gates, while demonstrating their use in various relevant quantum applications. Moreover, the difficult cubic gates may be chosen either relatively weak or all identical, thus facilitating potential experimental implementations.

From a practical point of view, this approach means that methods to optically realize the simplest, lowest-order non-Gaussian single-mode CV operation, which is the cubic phase gate [6], are sufficient to perform all kinds of advanced optical quantum information processing, including discrete-variable (DV), entangling gates on two standard photonic qubits, which are otherwise unavailable via only linear mode transformations. Note that it has been shown that naturally occurring “trisqueezed”

* nbudinge@t-online.de

† loock@uni-mainz.de

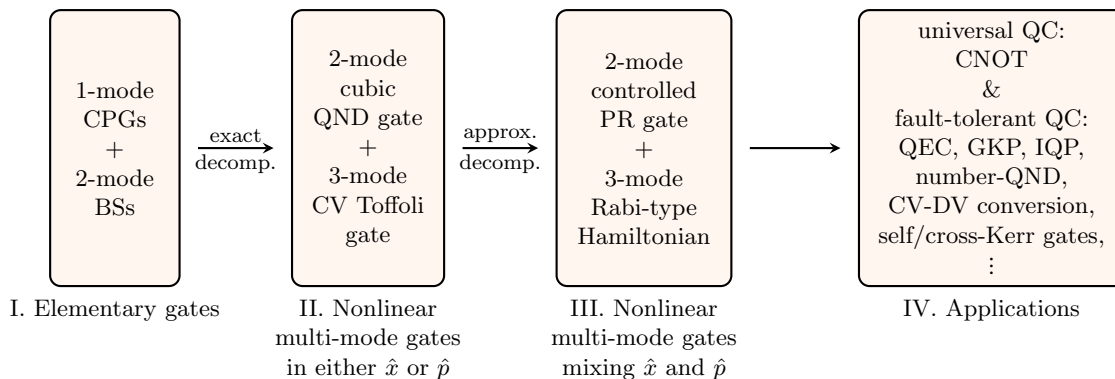


FIG. 1. Schematic illustration of the hybrid decomposition method for optical non-Gaussian gates. The acronyms are as follows. CPG, cubic phase gate; BS, beam splitter; QND, quantum nondemolition; PR, phase rotation; QC, quantum computation; QEC, quantum error correction; IQP, instantaneous quantum polynomial [18, 19]. Conversions between discrete and continuous variables (CV-DV conversion) can also be achieved with the help of Rabi-type Hamiltonian gates [20]. The gates of step II and III are given in equations (2) and (1), respectively.

states, which were experimentally already demonstrated in a nonoptical, superconducting platform [21], can be converted into cubic phase states, as typically used as a resource state to implement a cubic phase gate, via Gaussian operations [22].

More specifically, we show in this paper how certain elements of all-optical, fault-tolerant, and universal quantum computation can be implemented using primarily Gaussian resources together with cubic phase gates in reasonable numbers. Our approach is based on the efficient decomposition of two non-Gaussian CV multimode gates, namely the two-mode controlled phase rotation gate and the three-mode Rabi-type Hamiltonian gate

$$e^{i\alpha\hat{x}_1\hat{n}_2} \quad \text{and} \quad e^{i\beta\hat{x}_1\hat{\sigma}_{x,S}}, \quad (1)$$

respectively, where $\hat{\sigma}_{x,S}$ refers to spin operators as expressed by an optical Schwinger representation, i.e., one spin represented by two oscillator modes. As an intermediate set of multimode gates, we consider so-called two-mode cubic quantum nondemolition (QND) gates and three-mode CV Toffoli gates

$$e^{i\alpha\hat{x}_1\hat{x}_2^2} \quad \text{and} \quad e^{i\beta\hat{x}_1\hat{x}_2\hat{x}_3}, \quad (2)$$

respectively. These nonlinear multimode gates have the advantage that they do not mix the two phase-space variables x and p , thus allowing for an exact decomposition into single-mode cubic phase gates and beam splitters. In contrast, the finally obtained nonlinear multimode gates, as needed for our examples of important elements in photonic quantum information processing, do mix x and p , and so these require an additional approximation step.

Overall, our efficient decomposition method (see Fig. 1) then relies on a combination of exact decomposition techniques and approximate Trotterization – a kind of hybrid decomposition technique, which we show works remarkably well. We analyze the performance of these hybrid decompositions for a single-photon

two-qubit controlled- Z gate and for two distinct variants of an optical generation of various manifestations of Gottesman-Kitaev-Preskill (GKP) states [4]. Generally, we expect our decomposition method to be of potential use in various other applications, including those based on Kerr-type interactions. One example is a Kerr-interaction-based photon-number QND measurement in a completely transparent photon detector [23, 24], which, however, can also be realized directly via a cubic, two-mode controlled phase rotation gate, like that for which we derive efficient decompositions, $e^{i\alpha\hat{x}_1\hat{n}_2}$.

As for the non-Gaussian continuous-variable GKP state examples, our approach is highly compatible with concepts of measurement-based quantum computing with continuous-variable cluster states for which the single-mode cubic phase gate is the canonical non-Gaussian gate [11, 25]. In this case, the cubic elements may either be introduced on the level of the measurements, allowing to measure observables that are no longer linear combinations of x and p , i.e., going beyond Gaussian homodyne measurements, or on the level of the “off-line”-prepared cluster state by replacing some of the squeezed-vacuum-state nodes by cubic phase states – achieving universal continuous-variable “on-line” operations solely by means of Gaussian homodyne measurements. In the former case, the non-Gaussian measurements may be based on the detection of photon numbers, which is generally a common current approach to the engineering of non-Gaussian optical states, i.e., an approach similar to “Gaussian boson sampling” [26, 27] employing Gaussian squeezed-state resources, linear optics, and photon counting [28, 29].

Similarly, non-Gaussian states may then be directly realized within a Gaussian cluster state through photon number measurements [30]. A potentially useful feature of our approach, based on the lowest-order non-Gaussian states and gates, could be that in order to engineer these simplest nonlinear elements, for instance, via

non-Gaussian photon measurements, full photon-number resolution of the optical detectors up to a sufficiently high number may not be needed [6], similar to the results of Ref. [31], which, however, are still based on an approach close to Gaussian boson sampling.

With our approach, canonical cubic phase gates realized via a CV cluster state can be directly used to obtain standard GKP qubit states as well as GKP “magic states” within the cluster state, independent of photon measurements beyond the level of, for instance, cubic-phase-state generations. This would allow to obtain logical non-Clifford gates for GKP qubits via magic gate teleportation and nonlinear feedforward [7], despite the recent result that a single CV cubic gate acting directly upon a physical GKP qubit cannot provide a near-unity fidelity non-Clifford gate operation [32]. Alternatively, nonlinear gates diagonal in the number operator, such as those based on a quartic Kerr interaction, may be employed in order to obtain an efficient and robust non-Clifford gate for GKP qubits [33]. For this type of quartic gate our decomposition method into cubic and quadratic gates can also be used.

The paper is structured as follows. In Sec. II, we review the most important elements of the different approaches to optical quantum computing with a particular focus on single-photon qubits and GKP qubits. However, the latter will be introduced in a little more detail in the later section on applications of our methods, Sec. IV. Our methodology itself will be described in Sec. III. Sections V and VI include a brief discussion of the effects of photon loss on our schemes and a conclusion, respectively. Two extra appendices present more details on the calculations and the parameter optimizations.

II. OPTICAL QUANTUM COMPUTATION

Photons are robust to decoherence; however, they get easily lost, being reflected into the wrong path or even absorbed by the environment. Moreover, for photonic two-qubit gates based on standard photonic qubits, such as a CNOT or CZ gate, the necessary nonlinear interaction $\sim \pi \hat{n} \otimes \hat{n}$ is hard to obtain. In this section, we briefly review notions of universality and fault tolerance in the context of optical encodings and quantum error correction codes, including sophisticated “hardware-efficient”, highly nonclassical “bosonic codes”. In the CV setting, for processing quantum oscillators or “qumodes”, we briefly discuss known decomposition techniques as well as optical approaches to cubic-phase state and gate implementations as the lowest-order nonlinear resources to introduce a non-Gaussian element and complete the universal gate sets.

A. Universal quantum computation

Independent of a physical realization, there are various choices for encoding and processing quantum information. The most common one is that based on qubits and qudits, commonly referred to as DV approach. Another one is that exploiting continuous quantum variables, as, for instance, given in a quantized harmonic oscillator, typically referred to as a “qumode”. Such latter schemes, processing qumodes, are also known as CV quantum information processing or computing. In either approach, DV or CV, distinct models of universal quantum computing have been proposed, most notably the circuit model [9, 34] based on a reversible sequence of unitary gate operations and the measurement-based model [11, 35] based on an irreversible sequence of measurements performed on a universal, so-called cluster state.

In the context of DV quantum computing with qubits, the most common universal gate set, approximating, in principle, any multiqubit operation to arbitrary precision, is

$$\{\hat{H}, \hat{S}, \hat{T}, \text{CNOT}\}, \quad (3)$$

where \hat{H} is the Hadamard gate with $\hat{H}|0\rangle = (|0\rangle + |1\rangle)/\sqrt{2}$, $\hat{H}|1\rangle = (|0\rangle - |1\rangle)/\sqrt{2}$, and the other two single-qubit gates, $\hat{S} = \exp(-i\pi\hat{Z}/4)$ and $\hat{T} = \exp(-i\pi\hat{Z}/8)$, lead to rotations around the Z axis of the Bloch representation where \hat{Z} is a Pauli operator. The two-qubit CNOT gate applies a bit flip on the second, target qubit only when the first, control qubit is in the state $|1\rangle$.

Note that the set of Eq. (3) contains a redundant gate, $\hat{S} = \hat{T}^2$. It is, however, convenient to keep the gate \hat{S} in the universal set, because it allows to complete the set of so-called Clifford gates $\{\hat{H}, \hat{S}, \text{CNOT}\}$, which are known to be efficiently simulable by a classical computer [34]. Towards implementations and fault tolerance, it is useful to reserve the \hat{T} gate only for the non-Clifford part of a quantum computation, which is the crucial part to accomplish universality and to circumvent classical simulability for a “quantum advantage”. Not to waste non-Clifford gates for Clifford quantum computing becomes particularly striking in the CV case.

In this CV case, the most common universal gate set to process a multiqumode system and obtain a notion of universal CV quantum computing is

$$\{\hat{F}, e^{it\hat{x}}, e^{is\hat{x}^2}, e^{ir\hat{x}^3}, \text{CSUM}\}. \quad (4)$$

Using the convention $\hbar = 1$ throughout this paper, the Fourier gate \hat{F} is given by $\hat{F} = \exp\left(i\frac{\pi}{2}\frac{\hat{x}^2 + \hat{p}^2}{2}\right)$, allowing to switch between the position and momentum variables \hat{x} and \hat{p} , similar to a qubit Hadamard gate. The other single-qumode gates are $e^{it\hat{x}}$, generating momentum shifts, and the quadratic and cubic phase gates, $e^{is\hat{x}^2}$ and $e^{ir\hat{x}^3}$, respectively. The Gaussian quadratic gate involves a single-qumode phase rotation and “squeezing”.

The two-qumode gate $\text{CSUM} = e^{-i\hat{x}_1\hat{p}_2}$ plays the role of a CV entangling gate, analogous to the two-qubit CNOT, transforming the second, target qumode as $\hat{x}_2 \rightarrow \hat{x}_2 + \hat{x}_1$, the first, control qumode as $\hat{p}_1 \rightarrow \hat{p}_1 - \hat{p}_2$, while \hat{x}_1 and \hat{p}_2 remain invariant.

Note that both \hat{F} and CSUM are not diagonal in the x variable, whereas all the other gates are. The latter is useful to construct a model for CV measurement-based quantum computing with CV cluster states [11] and consequently the CSUM gate is also commonly replaced by CZ = $e^{i\hat{x}_1\hat{x}_2}$. The Fourier gate occurs naturally in CV cluster-state quantum computing via the elementary teleportations in the cluster state.

Similar to the discussion above for qubits, the set of Eq. (4) also contains a redundant gate, the quadratic phase gate $e^{is\hat{x}^2}$, which is obtainable from the cubic phase gate $e^{ir\hat{x}^3}$ [36], as pointed out in Refs. [37, 38]. However, it is preferred to keep the quadratic gate in the universal set, because it allows to complete the ‘‘Clifford set’’ for continuous variables, $\{\hat{F}, e^{it\hat{x}}, e^{is\hat{x}^2}, \text{CSUM}\}$. This nonuniversal gate set allows to perform any multi-qumode Gaussian operation, corresponding to all linear mode operator transformations generated by an arbitrary quadratic multimode Hamiltonian. Similar to the qubit case, there are efficient classical representations to simulate the Gaussian evolution of Gaussian multimode states [39].

Especially in the optics context, it is better to employ the non-Gaussian cubic gates as little as possible, and hence the Gaussian processing should be done entirely independent of cubic or any higher nonlinear gates. This minimal use of only the simplest nonlinear gate operations in optical implementations is one of the main motivations for the models in the present paper. Next, we shall briefly discuss the notions of quantum error correction and fault tolerance, before looking at the most common ways to combine all these abstract, implementation-independent concepts in all-optical, universal, and fault-tolerant quantum computing.

B. Quantum error correction and fault tolerance

The physical CV errors are continuous and hence the CV states can be subject to very small, diffusive errors. In fact, the most common and practically relevant qumode errors are Gaussian errors such as excitation loss or thermal noise. In the optics context, excitation loss means photon loss. Such Gaussian errors generally cannot be suppressed by employing quantum error correction codes that are solely based upon Gaussian states and operations [40, 41].

In the DV approach, sufficiently many physical qubits can be used to form one logical qubit and for the most common quantum error correction codes, known as stabilizer codes, the Clifford gate set $\{\hat{H}, \hat{S}, \text{CNOT}\}$ is sufficient to construct the logical qubit states as well as to

perform the error correction. In the CV setting, however, fault tolerance and effective quantum error correction require an additional discretization of the qumode. A very powerful and prominent code to achieve this is the so-called Gottesman-Kitaev-Preskill (GKP) code, encoding a logical qubit in a physical qumode. This approach is not only ‘‘hardware efficient’’, directly making use of the infinite-dimensional oscillator Hilbert space with no need for adding extra auxiliary states or modes unless the GKP qubit code is concatenated with standard multi-qubit codes for an enhanced error robustness [33, 42–48]. It also circumvents the no-go results on Gaussian CV quantum error correction, enabling one to detect small diffusive errors and correct them at the expense of a logical error, which then requires an additional higher-level multi-GKP-qubit stabilizer code. The syndrome measurement of the GKP code is a non-Gaussian operation, projecting on the GKP code and error spaces, which can be implemented by Gaussian operations together with the non-Gaussian GKP qubit ancilla states.

Thus, bosonic quantum error correction codes [49–54], and among them, in particular, the GKP code [4, 55], are an efficient means to protect quantum information embedded into a discretized code space against CV errors of the physical qumodes. The GKP code is resource efficient using only a single qumode and it only requires Gaussian operations for entangling and encoding qubits, which is of particular practical significance in optics for the photonic GKP code. It was shown recently that an extra non-Gaussian element, beyond that given by a supply of GKP qubits, is not even needed for full multiqubit universality [56, 57]. Later, as one possible application of our CV gate decompositions in the context of all-optical implementations, we will see that the non-Gaussian cubic phase gate $e^{ir\hat{x}^3}$, together with some initial Gaussian states, Gaussian homodyne measurements, Fourier, and beam-splitting operations, allows to generate GKP qubits. For the nonlinear cubic gate to be experimentally available, it may have to be weak. For it to be robustly implementable, it should not depend on its continuous, fully tunable operation. Preferred is a fixed cubic gate with a fixed interaction strength, for reasons that we discussed in this subsection. We shall address these issues in our GKP generation scheme.

C. Photonic codes and gates

The conceptually simplest way to encode a photonic qubit is to only make use of a two-dimensional subspace of an optical mode’s Hilbert space that is spanned by the vacuum and the single-photon states. More common and convenient than qubit superposition states of $|0\rangle$ and $|1\rangle$ in a single optical mode (single-rail) is to construct a qubit subspace $\{|1\rangle|0\rangle, |0\rangle|1\rangle\}$ on two optical modes (dual-rail). Typically, polarization or temporal modes are employed for such dual-rail photonic qubits. While all single-qubit gates on photonic dual-rail qubits can be re-

alized via linear mode transformations of the two modes, a two-qubit entangling gate cannot. Thus, from the universal gate set $\{\hat{H}, \hat{S}, \hat{T}, \text{CNOT}\}$, only CNOT is hard to obtain directly requiring a quartic, Kerr-type $\sim \pi \hat{n} \otimes \hat{n}$ interaction of sufficient strength $\sim \pi$. Applying the corresponding unitary gate $e^{i\pi \hat{n} \otimes \hat{n}}$ upon two optical modes with states $|0\rangle|0\rangle$, $|1\rangle|0\rangle$, $|0\rangle|1\rangle$, or $|1\rangle|1\rangle$ only gives a sign flip for the input state $|1\rangle|1\rangle$ and otherwise acts as the identity – a CZ gate. Together with 1-qubit Hadamard gates, on two-mode qubits simply implementable as a beam splitter, one can construct a CNOT gate from this. The CZ then acts upon modes 2 and 4 of the two dual-rail input qubits encoded into modes 1, 2 and 3, 4, respectively.

Thus, efficient photonic quantum computation based on single-photon qubits, each encoded into two modes, if directly implemented in a unitary circuit model, would depend on the availability of a robust, loss-tolerant, sufficiently strong, nonlinear two-mode gate. An alternative is a single-mode, nonlinear or Kerr-type gate $\sim \pi \hat{n}^2$ of similar strength $\sim \pi$ in combination with beam splitters [3, 58], which can either provide a near-deterministic, heralded nonlinear single-mode gate or correspond to a, in principle deterministic, quartic CV single-mode interaction gate. We will see that our CV gate decompositions allow to obtain photonic two-qubit entangling gates from single-mode cubic phase gates.

Probabilistic nonlinear gates can be combined with gate teleportation techniques. In fact, to circumvent the “on-line” implementation of a photon-photon CNOT gate, measurement-based schemes have been proposed making use of multiphoton ancilla states [3], for instance, in the form of cluster states [35, 59, 60]. The entangling gates to build a sufficiently large cluster state “off-line” may then be probabilistic. Similar approaches can be used in order to incorporate quantum error correction codes and a notion of loss and even fault tolerance into the schemes [61]. Nonetheless, for a large-scale quantum computer, besides the experimental complication of multiplexing and at least short-term storage of quantum information, a large resource overhead is expected. In a DV time-domain approach, high experimental source clock rates, for example using quantum dots, are a promising element to create this overhead in a practical fashion.

A more direct approach would be based on processing continuous variables, i.e., the mode’s continuous degrees of freedom. In quantum optics this is typically done by relating the in- and out-of-phase amplitudes of the electromagnetic field to the quadrature operators \hat{x} and \hat{p} . Then the Gaussian gates, $\{\hat{F}, e^{it\hat{x}}, e^{is\hat{x}^2}, \text{CSUM}\}$, can be efficiently realized experimentally. The quadratic phase gate can be replaced by an optical, single-mode squeezing operation $e^{is(\hat{x}\hat{p}+\hat{p}\hat{x})}$ and CSUM may be substituted by an optical beam splitter $e^{i\theta(\hat{p}_1\hat{x}_2-\hat{x}_1\hat{p}_2)}$ as it is decomposable into beam splitters and single-mode squeezers [62]. In contrast, the non-Gaussian, single-mode cubic phase gate to achieve CV universality $e^{ir\hat{x}^3}$ is more difficult to obtain, requiring a nonlinear optical mode transformation.

We shall address this in Sec. II E. Note that the Gaussian entangling gates, CSUM or a beam splitter, are, unlike the CNOT gate for single-photon qubits, relatively easy to implement. Other optical CV encodings exist as well, most notably utilizing the continuous time-frequency degrees of freedom. Here, non-Gaussian operations as well as GKP states have been experimentally demonstrated [63, 64]; however, performing interactions between modes remains challenging, exhibiting a closer resemblance to the DV than to the CV approaches described above.

Conceptually different from a direct processing of logical, CV quantum information is to encode logical DV states or especially qubits into physical, optical CV systems. This leads to new possibilities of photonic quantum information processing, in particular, in the context of quantum error correction, but also to new types of complications. Below, when discussing various applications of our approach, we will consider the GKP code, which as an instance of a shift-invariant bosonic code is an example of such a photonic code. Its optical manipulation is based on a translation of the CV quantum optical gate operations into logical gates acting on the GKP code space. This results, in principle, in a higher level of scalability, especially when the modes to be processed are primarily defined in the time domain [1, 2]. The GKP states are still hard to obtain on demand, but nonetheless allow for a loss- and fault-tolerant processing that goes beyond simple quantum error detection and allows for photonic quantum error correction. Particularly attractive is that the use of efficient Gaussian two-mode gates for entangling two qumodes from the CV setting directly translates to GKP qubits and their logical CNOT gates. However, single-qubit universality for GKP qubits is harder than that for single-photon qubits, requiring nonlinear mode operator transformations. Next let us take a look at the most common methods for gate decomposition.

D. Gate decomposition techniques

In the year 1999, Lloyd and Braunstein demonstrated that every multimode operation could, in principle, be approximated to arbitrary precision using only gates from the universal gate set of Eq. (4) [9]. However, for the experimental feasibility of a given operation, the number of elementary gates required for its approximation is no less important. Consequently, various CV gate decomposition schemes have been developed enabling certain groups of qumode operations to be implemented more efficiently. We shall briefly discuss the Trotter-Suzuki decomposition [65, 66], the commutator-based approach proposed by Lloyd and Braunstein [9] and optimized in Ref. [38], as well as the exact gate decomposition scheme [67] as developed in Ref. [68]. An efficient and exact decomposition of Gaussian operations can be found in Ref. [69] adapted to CV cluster computation.

The Trotter-Suzuki decomposition can be used to ob-

tain the operation $e^{it(\hat{A}+\hat{B})}$ from the two gates $e^{it\hat{A}}$ and $e^{it\hat{B}}$. It relies upon the Lie-Trotter product formula,

$$\left(e^{i\frac{t}{n}\hat{A}}e^{i\frac{t}{n}\hat{B}}\right)^n \xrightarrow{n \rightarrow \infty} e^{it(\hat{A}+\hat{B})}. \quad (5)$$

By introducing and adapting individual gate strengths t_i of the n repetitions, the order of convergence can be chosen arbitrarily high as shown in Refs. [65, 66]. Similarly, in the commutator-based decomposition schemes [9, 38], the operator $e^{t[\hat{A},\hat{B}]}$ is approximated using the relation

$$\left(e^{-i\sqrt{t/n}\hat{A}}e^{-i\sqrt{t/n}\hat{B}}e^{i\sqrt{t/n}\hat{A}}e^{i\sqrt{t/n}\hat{B}}\right)^n \xrightarrow{n \rightarrow \infty} e^{t[\hat{A},\hat{B}]}, \quad (6)$$

given the operators $e^{it\hat{A}}$ and $e^{it\hat{B}}$. Repeating this procedure then also enables the creation of operations with nested commutators. In combination with the Trotter-Suzuki decomposition and the universal gate set, this then allows for the implementation of any polynomial of the bosonic mode operators \hat{x}_i and \hat{p}_i and hence any multi-qumode operation [9]. Again, by adapting the gate strengths t_i of the different repetitions, the order of convergence can be increased which significantly enhances the efficiency of the decomposition when targeting large gate strength t along with high accuracies. Nevertheless, the number of approximate steps needed to arrive at the desired operation lets the amount of required elementary gates rise rapidly. Therefore, whenever possible the exact decomposition of gates is preferable.

The exact gate decomposition scheme by KalaJdziewski and Arrazola [68] enables the decomposition of operators of the general form

$$\exp\left(it\left(\prod_{j=1}^{N-1}\hat{x}_j\right)\hat{x}_N^n\right), \quad (7)$$

where N as well as $n \cdot N$ must be divisible by either two or three. As this is based on the relation [38, 68, 70]

$$e^{i\alpha\hat{x}_j^m\hat{p}_k}e^{it\hat{x}_j^n}e^{-i\alpha\hat{x}_j^m\hat{p}_k} = e^{it(\hat{x}_k+\alpha\hat{x}_j^m)^n} \quad (8)$$

and the eventual cancellation of unwanted polynomial terms of the right-hand side, the optical position and momentum operators \hat{x}_i and \hat{p}_i must not be mixed. Hence, the subgroup of exactly decomposable gates is rather small. Nevertheless, if a given quantum operator is in the form of Eq. (7), its exact decomposition is generally superior to approximate approaches in gate count and accuracy.

E. Optical cubic phase states and gates

The hardest gate of the universal gate set of Eq. (4) to realize quantum optically is the single-mode cubic phase gate [4], $e^{ir\hat{x}^3}$, which is the only non-Gaussian gate of the set. It acts trivially on the position operator, $e^{-ir\hat{x}^3}\hat{x}e^{ir\hat{x}^3} = \hat{x}$, while the momentum operator is transformed by it in a nonlinear fashion [37],

$$e^{-ir\hat{x}^3}\hat{p}e^{ir\hat{x}^3} = \hat{p} + 3r\hat{x}^2, \quad (9)$$

shifting the momentum by the squared position [71]. This gate was originally introduced as one option to add a non-Clifford element and complete the logical universal gate set for GKP qubits [4]. We will come back to this later. While the gate is also the canonical choice to achieve CV universality, it is particularly well suited to incorporate a non-Gaussian element into the concept of CV cluster computation [11, 25]. Earlier it was considered in another variant of measurement-based quantum computation, namely a version of CV optical gate teleportation [5].

The original idea to optically obtain a cubic phase gate was based on photon measurements on parts of Gaussian states [4, 25, 28], which conditionally prepares a cubic phase state $\int dx e^{irx^3}|x\rangle$ that can be used as a resource for cubic-phase-gate teleportation. Alternatively, small-number Fock superposition states, being approximations of cubic phase states, may be directly used as single-mode ancilla states for weak cubic-phase-gate teleportation [72]. Later, the concept of nonlinear squeezing was introduced, which is related to the non-Gaussian and nonclassical properties of a nonlinear, cubic phase state [73]. The higher the nonlinear squeezing, corresponding to a higher average number of photons, the stronger the cubic phase gate becomes that can be obtained with the help of the approximated cubic phase state. Eventually, it was shown that nonlinear feedforward operations based on the results obtained from homodyne detectors allow to effectively measure nonlinear quadrature combinations. Combined with the nonclassical photon ancilla states, this offers an efficient way to optically realize a single-mode cubic phase gate [6]. The technique of nonlinear feedforward can also be employed to achieve magic gate teleportation using magic states for GKP qubits [7].

Most recently, the nonlinear feedforward operation for cubic phase gate teleportation was experimentally demonstrated [8]. The degree of nonlinear squeezing of the non-Gaussian ancilla state experimentally achieved is related to the cubic phase gate strength parameter r in Eq. (9) as $r \approx 0.17$. An ancilla state with a higher photon number would exhibit larger nonlinear squeezing, and this can be used to make the resulting cubic phase gate stronger. We will show that our decomposition method, when applied and optimized for GKP state generation of fairly high fidelity above 90% using single-mode cubic phase gates and beam splitters, yields parameter values all below $r = 0.17$. Thus, our decomposition-based scheme is fully compatible with the recent experimental nonlinear-feedforward demonstration. In order to achieve better fidelities, we would apply a larger sequence of gates where each gate is typically even weaker. The remaining complication in a practical application of these schemes would be loss and noise as well as relatively low gate fidelities, so that a smaller sequence of imperfect gates is preferable. We leave a complete analysis of the experimental scheme of Ref. [8], including loss and imperfections, applied to our gate decompositions for, especially, GKP state generation to future work. The important

conclusion here is that the methods of Refs. [6–8, 72, 73] can be very well combined with our present approach.

III. HYBRID DECOMPOSITION SCHEME FOR OPTICAL NON-GAUSSIAN GATES

The basis of all subsequent considerations is the universal gate set given by

$$\left\{ e^{i\pi(\hat{x}^2+\hat{p}^2)}, e^{it\hat{x}}, e^{is(\hat{x}\hat{p}+\hat{p}\hat{x})}, e^{i\theta(\hat{p}_1\hat{x}_2-\hat{x}_1\hat{p}_2)}, e^{ir\hat{x}^3} \right\} \quad (10)$$

with $t, s, \theta, r \in \mathbb{R}$ and the quadrature operators $\hat{x}_k = \frac{1}{\sqrt{2}}(\hat{a}_k + \hat{a}_k^\dagger)$ and $\hat{p}_k = \frac{1}{\sqrt{2}i}(\hat{a}_k - \hat{a}_k^\dagger)$. The Gaussian operations, namely phase rotation, displacement, squeezing, and beam splitting are all readily available in experimental quantum optics, as discussed in Sec. II. The cubic phase gate, on the other hand, is experimentally more challenging to implement, but also for this very recent demonstrations exist, as described in Sec. II E.

Using only gates from this set we want to approximate two multimode gates, the controlled phase rotation gate $e^{i\alpha\hat{x}_1\hat{n}_2}$ and the Rabi-type-Hamiltonian gate $e^{i\beta\hat{x}_1\hat{\sigma}_{x,s}}$, where the latter refers to spin operators as expressed by an optical Schwinger representation, i.e., one spin represented by two oscillator modes. Both types of gates can be used to achieve universal quantum computing in an optical setting, as we will see later. As the given gate set is universal, it is possible to approximate any multimode quantum gate using only a finite number of gates from the set. However, the experimental feasibility of any gate approximation depends heavily on the amount of concatenated gates. Hence the focus of this paper lies on obtaining good approximations while also minimizing the number of basic operations needed.

To achieve this, we use a hybrid decomposition approach, which is based on exact decomposition schemes followed by one step of the approximation technique known as Trotterization, as illustrated in Fig. 1. This way, we are able to decompose nonlinear multimode gates, which mix \hat{x} and \hat{p} while still utilizing the low gate counts and unit fidelities of exact decompositions. While the general efficiency of a gate decomposition is difficult to quantify as it depends on the specific application as well as the required accuracy, we presume this combination of exact decompositions with only one approximate step to be generally more efficient than commutator-based approximations. Let us now discuss these individual techniques.

A. Exact decomposition of cubic multimode gates

The first step of the presented approximation scheme is the exact decomposition of two cubic multimode gates, namely the cubic QND gate $e^{i\alpha\hat{x}_1\hat{x}_2^2}$ and the CV Toffoli gate $e^{i\beta\hat{x}_1\hat{x}_2\hat{x}_3}$. These gates will be the basic elements of the following Trotterization. Using a lemma to the

TABLE I. Comparison of the number of elementary gates needed for the exact decomposition of the cubic QND gate $e^{i\alpha\hat{x}_1\hat{x}_2^2}$ and the CV Toffoli gate $e^{i\beta\hat{x}_1\hat{x}_2\hat{x}_3}$ with the corresponding gate counts from Kalajdziewski *et al.* [68]. The quadratic QND gates required in [68] are either CZ or CSUM gates.

Target gate	Present paper		Kalajdziewski <i>et al.</i>	
	Cubic phase gates	Beam splitters	Cubic phase gates	QND gates
Cubic QND	3	3	5	4
CV Toffoli	4	9	7	10

Baker-Campbell-Hausdorff formula,

$$e^{\hat{A}}\hat{B}e^{-\hat{A}} = \sum_{n=0}^{\infty} \frac{1}{n!} \underbrace{[\hat{A}, [\hat{A}, \dots [\hat{A}, \hat{B}] \dots]]}_n, \quad (11)$$

and the beam splitter $\hat{B}_{kl}(s) = e^{is(\hat{p}_k\hat{x}_l - \hat{x}_k\hat{p}_l)}$, we easily obtain

$$\hat{B}_{12}(s)\hat{x}_1\hat{B}_{12}(-s) = \cos(s)\hat{x}_1 + \sin(s)\hat{x}_2, \quad (12)$$

and thus

$$\begin{aligned} & \hat{B}_{12}(s)e^{ir\hat{x}_1^3}\hat{B}_{12}(-2s)e^{ir\hat{x}_1^3}\hat{B}_{12}(s) \\ &= e^{ir(\cos(s)\hat{x}_1 + \sin(s)\hat{x}_2)^3} e^{ir(\cos(s)\hat{x}_1 - \sin(s)\hat{x}_2)^3} \\ &= e^{2ir\cos^3(s)\hat{x}_1^3} e^{6ir\cos(s)\sin^2(s)\hat{x}_1\hat{x}_2^2}. \end{aligned} \quad (13)$$

This leads us to the exact decomposition of a cubic QND gate,

$$e^{i\alpha\hat{x}_1\hat{x}_2^2} = \hat{B}_{12}(s)e^{ir\hat{x}_1^3}\hat{B}_{12}(-2s)e^{ir\hat{x}_1^3}\hat{B}_{12}(s)e^{-i\beta\hat{x}_1^3}, \quad (14)$$

with $\alpha = 6r\cos(s)\sin^2(s)$ and $\beta = 2r\cos^3(s)$ using a total of three single-mode cubic phase gates and three beam splitters. Continuing with the result of Eq. (14) we directly obtain

$$\begin{aligned} & \hat{B}_{23}(u)e^{it\hat{x}_1\hat{x}_2^2}\hat{B}_{23}(-2u)e^{-it\hat{x}_1\hat{x}_2^2}\hat{B}_{23}(u) \\ &= e^{it\hat{x}_1(\cos(u)\hat{x}_2 + \sin(u)\hat{x}_3)^2} e^{-it\hat{x}_1(\cos(u)\hat{x}_2 - \sin(u)\hat{x}_3)^2} \\ &= e^{4it\sin(u)\cos(u)\hat{x}_1\hat{x}_2\hat{x}_3} = e^{2it\sin(2u)\hat{x}_1\hat{x}_2\hat{x}_3}. \end{aligned} \quad (15)$$

Note that the last term of Eq. (14) can be omitted in the above calculation. Hence we get a CV Toffoli gate at the expense of four single-mode cubic phase gates and nine beam splitters. In comparison to existing exact decomposition schemes [68] this not only reduces the number of especially single-mode cubic phase gates, but it also works using only simple beam splitters instead of the experimentally more challenging quadratic QND gates that involve additional squeezing operations. Table I lists the number of elementary gates needed for the exact decompositions of [68]. Note that the name CV Toffoli gate is usually assigned to the gate $e^{i\beta\hat{x}_1\hat{x}_2\hat{p}_3}$ instead of the gate

$e^{i\beta\hat{x}_1\hat{x}_2\hat{x}_3}$ used in this paper. Analogous to a DV three-qubit Toffoli gate, which applies a bit flip to the third qubit only when the two first qubits are both in the logical state $|1\rangle$, this commonly defined CV Toffoli gate shifts the position of mode 3, \hat{x}_3 , by an amount proportional to the product of the positions of modes 1 and 2, $\hat{x}_1\hat{x}_2$. However, both definitions only differ by a Fourier gate, which is easily implemented optically.

B. Efficient Trotter-Suzuki decomposition of the controlled phase rotation gate

Concatenating several cubic QND gates, while Fourier transforming the second mode of every second gate, we obtain

$$S_{\lambda}(t) = \prod_{j=1}^m \exp\left(it\lambda_j\hat{x}_1\frac{\hat{x}_2^2}{2}\right) \exp\left(it\mu_j\hat{x}_1\frac{\hat{p}_2^2}{2}\right), \quad (16)$$

with the indexation of the product going from right to left and $\lambda = (\lambda_m, \mu_m, \dots, \lambda_1, \mu_1)^T$. The first-order Trotter-Suzuki decomposition is then given by the Lie-Trotter product formula

$$\exp\left(i\alpha\hat{x}_1\frac{\hat{x}_2^2 + \hat{p}_2^2}{2}\right) = \left[S_{(1,1)^T}\left(\frac{\alpha}{b}\right)\right]^b + \mathcal{O}\left(\frac{1}{r}\right), \quad (17)$$

with $b \in \mathbb{N}$. Higher orders of convergence can be achieved by using specific sets of parameters λ as provided by Suzuki in Refs. [65, 66]. However, for small b the order of convergence should not surpass its role of guidance: As demonstrated in Ref. [74], finding the right set of parameters for a specific problem instead of using the common Trotter-Suzuki decompositions can significantly enhance the approximation. But before we can attempt such a parameter optimization, we need to determine the impact of different parameter sets λ on the different applications. In order to do this analytically, a change in representation will prove to be useful:

Let us regard the impact of the operator on the different quadratures of the two modes. Note that, up to a global phase, this defines an arbitrary operator unambiguously (see Appendix A). Starting with the second mode and using $e^{i\frac{t}{2}\hat{x}^2}\hat{p}e^{-i\frac{t}{2}\hat{x}^2} = \hat{p} - t\hat{x}$ and $e^{i\frac{t}{2}\hat{p}^2}\hat{x}e^{-i\frac{t}{2}\hat{p}^2} = \hat{x} + t\hat{p}$, it is easily seen that

$$\begin{aligned} S_{\lambda}^b(t)\hat{x}_2S_{\lambda}^b(-t) &= P_{xx}[t\hat{x}_1]\hat{x}_2 + P_{xp}[t\hat{x}_1]\hat{p}_2, \\ S_{\lambda}^b(t)\hat{p}_2S_{\lambda}^b(-t) &= P_{px}[t\hat{x}_1]\hat{x}_2 + P_{pp}[t\hat{x}_1]\hat{p}_2. \end{aligned} \quad (18)$$

The thereby defined polynomials P_{xx} , P_{xp} , P_{px} , and P_{pp} are all of the order $2mb \equiv L$ and can easily be calculated for a given λ . The corresponding recursive formulas are presented in Appendix A.

While the operator's impact on the first mode's quadratures is slightly more complex, it is also solely dependent on these four polynomials. Consequently, P_{xx} , P_{xp} , P_{px} , and P_{pp} define the approximated controlled

phase rotation gate up to a global phase and provide an equal yet far more intuitive representation of S_{λ}^b than λ and b : the operator S_{λ}^b approximates the controlled phase rotation gate $e^{it\hat{x}_1\hat{n}_2}$ with

$$\begin{aligned} e^{it\hat{x}_1\hat{n}_2}\hat{x}_2e^{-it\hat{x}_1\hat{n}_2} &= \cos(t\hat{x}_1)\hat{x}_2 + \sin(t\hat{x}_1)\hat{p}_2, \\ e^{it\hat{x}_1\hat{n}_2}\hat{p}_2e^{-it\hat{x}_1\hat{n}_2} &= -\sin(t\hat{x}_1)\hat{x}_2 + \cos(t\hat{x}_1)\hat{p}_2 \end{aligned} \quad (19)$$

if and only if the four polynomials approximate the four functions cosine, sine, -sine, and cosine, respectively. The best approximation for a given L is thus obtained by simply choosing the truncated Taylor expansions of sine and cosine. Following directly from the recursive formulas is also the common as well as useful relation

$$P_{xx}[t]P_{pp}[t] - P_{xp}[t]P_{px}[t] = 1, \quad \forall t \in \mathbb{R}. \quad (20)$$

C. Decomposition of the Rabi-type Hamiltonians

The Trotter-Suzuki decomposition of the Rabi-type Hamiltonian gate $e^{i\alpha\hat{x}_1\hat{\sigma}_{x,S}}$ works rather similar. When replacing the cubic QND gates with CV Toffoli gates we obtain the operator

$$T_{\lambda}(t) = \prod_{j=1}^m \exp(it\lambda_j\hat{x}_1\hat{x}_2\hat{x}_3) \exp(it\mu_j\hat{x}_1\hat{p}_2\hat{p}_3), \quad (21)$$

with the indexation of the product going from right to left and $\lambda = (\lambda_m, \mu_m, \dots, \lambda_1, \mu_1)^T$ as before. Using modes 2 and 3 as a dual-rail qubit

$$\beta|0\rangle_{\text{DR}} + \gamma|1\rangle_{\text{DR}} = \beta|1\rangle_2|0\rangle_3 + \gamma|0\rangle_2|1\rangle_3, \quad (22)$$

together with the Schwinger representation of the Pauli operator

$$\hat{\sigma}_{x,S} = \hat{a}_2^\dagger\hat{a}_3 + \hat{a}_3^\dagger\hat{a}_2 \quad (23)$$

the Rabi-type Hamiltonian gate can be written as

$$e^{i\alpha\hat{x}_1\hat{\sigma}_{x,S}} = e^{i\alpha\hat{x}_1(\hat{a}_2^\dagger\hat{a}_3 + \hat{a}_3^\dagger\hat{a}_2)} = e^{i\alpha\hat{x}_1(\hat{x}_2\hat{x}_3 + \hat{p}_2\hat{p}_3)}, \quad (24)$$

and from the Lie-Trotter product formula it follows that

$$\left[T_{(1,1)^T}\left(\frac{\alpha}{b}\right)\right]^b \xrightarrow{b \rightarrow \infty} e^{i\alpha\hat{x}_1(\hat{x}_2\hat{x}_3 + \hat{p}_2\hat{p}_3)} = e^{i\alpha\hat{x}_1\hat{\sigma}_{x,S}}. \quad (25)$$

Furthermore, with similar impact on the different quadratures,

$$\begin{aligned} T_{\lambda}^b(t)\hat{x}_2T_{\lambda}^b(-t) &= P_{xx}[t\hat{x}_1]\hat{x}_2 + P_{xp}[t\hat{x}_1]\hat{p}_3, \\ T_{\lambda}^b(t)\hat{p}_2T_{\lambda}^b(-t) &= P_{px}[t\hat{x}_1]\hat{x}_3 + P_{pp}[t\hat{x}_1]\hat{p}_2, \\ T_{\lambda}^b(t)\hat{x}_3T_{\lambda}^b(-t) &= P_{xx}[t\hat{x}_1]\hat{x}_3 + P_{xp}[t\hat{x}_1]\hat{p}_2, \\ T_{\lambda}^b(t)\hat{p}_3T_{\lambda}^b(-t) &= P_{px}[t\hat{x}_1]\hat{x}_2 + P_{pp}[t\hat{x}_1]\hat{p}_3, \end{aligned} \quad (26)$$

the same polynomials as before, P_{xx} , P_{xp} , P_{px} , and P_{pp} can be used to define the approximated Rabi-type Hamiltonian gate up to a global phase (see Appendix A).

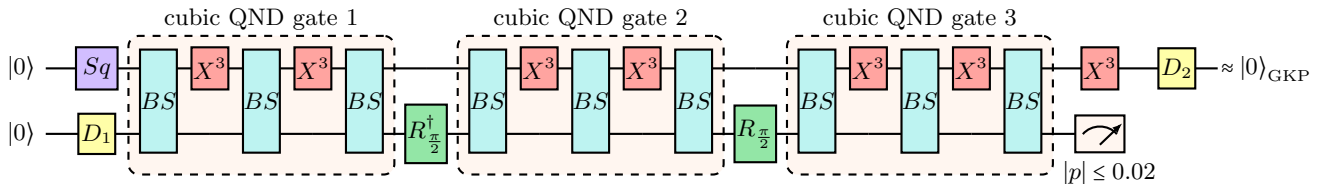


FIG. 2. Exemplary implementation of the presented hybrid decomposition scheme. Three exactly decomposed cubic QND gates are concatenated and their gate strengths are optimized based on the Trotter-Suzuki decomposition. Using an off-line squeezing of 12.2 dB (violet), two displacements (yellow), two Fourier gates (green), nine beam splitters (blue), seven cubic phase gates (red), and a conditional homodyne measurement with a success probability of 0.2% gives a $|0\rangle_{\text{GKP}}$ state with a fidelity of $\geq 90.5\%$. Explicit gate strengths can be found in Appendix B.

Note that with the Schwinger representation of the remaining Rabi-type Hamiltonian gates,

$$e^{i\alpha\hat{x}_1\hat{\sigma}_y, S} = e^{i\alpha\hat{x}_1(i\hat{a}_3^\dagger\hat{a}_2 - i\hat{a}_2^\dagger\hat{a}_3)} = e^{i\alpha\hat{x}_1(\hat{x}_2\hat{p}_3 - \hat{p}_2\hat{x}_3)}, \quad (27)$$

$$e^{i\alpha\hat{x}_1\hat{\sigma}_z, S} = e^{i\alpha\hat{x}_1(\hat{a}_2^\dagger\hat{a}_2 - \hat{a}_3^\dagger\hat{a}_3)} = e^{i\alpha\hat{x}_1\frac{\hat{x}_2^2 + \hat{p}_2^2}{2} - i\alpha\hat{x}_1\frac{\hat{x}_3^2 + \hat{p}_3^2}{2}}, \quad (28)$$

it is easily seen that the operators $S_\lambda(t)$ and $T_\lambda(t)$ are sufficient to approximate the full set of Rabi-type Hamiltonian gates. More precisely, we have

$$\hat{F}_3 \left[T_{(1,1)T} \left(\frac{\alpha}{b} \right) \right]^b \hat{F}_3^\dagger \xrightarrow{b \rightarrow \infty} e^{i\alpha\hat{x}_1(\hat{x}_2\hat{p}_3 - \hat{p}_2\hat{x}_3)}, \quad (29)$$

$$\left[S_{(1,1)T}^{(1,2)} \left(\frac{\alpha}{b} \right) S_{(1,1)T}^{(1,3)} \left(-\frac{\alpha}{b} \right) \right]^b \xrightarrow{b \rightarrow \infty} e^{i\alpha\hat{x}_1\frac{\hat{x}_2^2 + \hat{p}_2^2 - \hat{x}_3^2 - \hat{p}_3^2}{2}}, \quad (30)$$

with the Fourier transform $\hat{F}_3 = \exp(i\frac{\pi}{2}\frac{\hat{x}_2^2 + \hat{p}_2^2}{2})$ and the superscripts of S_λ here and in the following denoting on which modes the gates act upon. As an overall result, we have effectively obtained an efficient decomposition of general Rabi-type Hamiltonian gates based on CV Toffoli gates and their exact decompositions into a set of elementary CV operations that solely contains single-mode cubic phase gates and beam splitters. Though an approximation, in principle, this allows to deterministically simulate a general Rabi-type Hamiltonian interaction by optical means [75].

D. Optimizing the Trotter-Suzuki decomposition for different applications

One advantage of focusing on the four polynomials, as introduced above, is the simplicity with which they allow us to check for the order of convergence of the approximations. As the Taylor expansions of sine and cosine are well known, a simple comparison of all terms of corresponding order is sufficient. Consequently, the order of convergence n of a parameter set λ is coupled to a system of equations

$$\sum_{0 \leq k_1 \leq l_1 < k_2 \leq l_2 < \dots < k_n \leq l_n} \overbrace{\mu_{k_1} \lambda_{l_1} \mu_{k_2} \lambda_{l_2} \dots}^n = \sum_{0 \leq l_1 < k_2 \leq l_2 < k_3 \leq \dots < k_n \leq l_n} \overbrace{\lambda_{l_1} \mu_{k_2} \lambda_{l_2} \mu_{k_3} \dots}^n = \frac{1}{n!}, \quad (31)$$

where the left-hand side gives the two nonzero coefficients of n th order of the four polynomials and the right-hand side the corresponding coefficient of sine and cosine. While the common Trotter-Suzuki decomposition builds upon the symmetric operator $S_{(\frac{1}{2}, 1, \frac{1}{2}, 0)}$ resulting in only even orders of convergence, this allows us to also test *odd orders*. For example, the third order, after choosing its one degree of freedom appropriately, was found to be superior to comparable even orders in many of the applications tested in the scope of this paper. On the other hand, leaving the restrictions of Eq. (31) behind and conducting a free parameter search significantly improved results further. Therefore, unless stated otherwise, all presented approximations are optimized using the Basin-hopping algorithm as implemented by SciPy with starting points fulfilling Eq. (31), maximizing the fidelity to the respective target state. The explicit sets of parameters λ can be found in Appendix B.

The two separate steps of the hybrid decomposition scheme are illustrated in Fig. 2, where three exactly decomposed cubic QND gates are concatenated with optimized gate strengths in order to approximate a GKP state. Such GKP state generations are one of the possible applications of our method, which we shall treat in more detail next.

IV. APPLICATIONS

A. Approximating the qubit CZ gate

As a first application of our method we are going to look at a controlled- Z gate for photonic qubits, realizable via the two-mode gate $e^{i\pi\hat{n}_1\hat{n}_2}$. While single-qubit operations on photonic qubits are easily implemented experimentally using the gates from the universal gate set, as discussed in Sec. II, an additional two-qubit entangling gate is needed to achieve universality. For this, there are various approaches [3, 58–60], and already several experimental demonstrations too [76–83], which typically, however, are either destructive or heralded and probabilistic.

On the other hand, the two-mode interaction for a

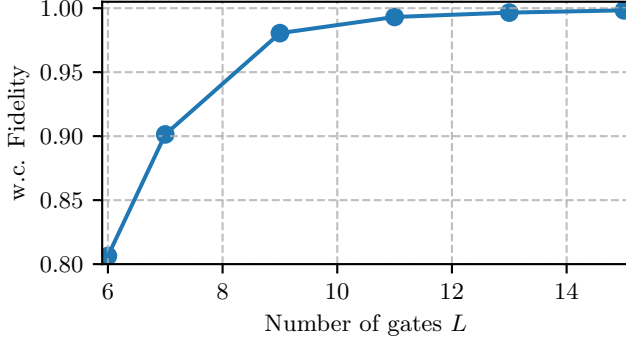


FIG. 3. Worst-case fidelity F_{wc} of the approximated controlled- Z gate for optimized parameter sets λ of different length L .

controlled- Z gate can be decomposed as

$$e^{i\pi\hat{n}_1\hat{n}_2} = e^{i\sqrt{\pi}\hat{x}_a\hat{n}_1} e^{-i\sqrt{\pi}\hat{p}_a\hat{n}_2} e^{-i\sqrt{\pi}\hat{x}_a\hat{n}_1} e^{i\sqrt{\pi}\hat{p}_a\hat{n}_2}, \quad (32)$$

with the subscript a denoting an extra ancilla mode. Combining the approximated controlled phase rotation gate $S_\lambda(t)$ with a displacement gate,

$$\hat{M}^{(j)} := e^{-i\sqrt{\pi}\hat{x}_a/2} S_\lambda^{(a,j)}(\sqrt{\pi}) \approx e^{i\sqrt{\pi}\hat{x}_a\hat{n}_j}, \quad (33)$$

we can thus approximate the controlled- Z gate by simply applying the same gate four times,

$$e^{i\pi\hat{n}_1\hat{n}_2} \approx \hat{M}^{(1)} \hat{F}_a^\dagger \hat{M}^{(2)} \hat{F}_a^\dagger \hat{M}^{(1)} \hat{F}_a^\dagger \hat{M}^{(2)} \hat{F}_a^\dagger. \quad (34)$$

Here the Fourier gate $\hat{F}_a = \exp(i\frac{\pi}{2}\frac{\hat{x}_a^2 + \hat{p}_a^2}{2})$ is performed on the ancilla and the superscripts indicate the different qubits and qumodes the operators act upon. A simple calculation shows that the four displacements combined just perform the operation $\hat{F}_1^\dagger \hat{F}_2^\dagger$ and can thus be replaced by two additional Fourier gates. In order to evaluate the quality of the approximated controlled- Z gate, we use the worst-case fidelity after tracing out the ancillary mode,

$$F_{wc} = \min_{|\psi\rangle, |\phi\rangle} F(\text{tr}_a [\text{CZ}_{\approx} |0\rangle_a |\psi\rangle_1 |\phi\rangle_2], \text{CZ} |\psi\rangle_1 |\phi\rangle_2), \quad (35)$$

$$|\psi\rangle, |\phi\rangle \in \{\alpha|0\rangle + \beta|1\rangle \mid |\alpha|^2 + |\beta|^2 = 1\},$$

with the fidelity of a density matrix and a pure state

$$F(\hat{\rho}, |\chi\rangle) = \langle \chi | \hat{\rho} | \chi \rangle. \quad (36)$$

In Fig. 3 this worst-case fidelity is calculated for optimized parameter sets λ of different length L . The exact number of the different elementary gates and the maximal required cubic phase gate strength can be found in Table II. The explicit parameter sets as well as the numerical calculations can be found in the Appendix.

The results show that it is possible to achieve a high-fidelity controlled- Z gate with close to ten cubic QND gates. Provided a source of deterministic single-mode

TABLE II. Number of elementary gates, required cubic phase gate strength r_{max} and worst-case fidelity F_{wc} of the approximated controlled- Z gate given by Eq. (34) for the optimized parameter sets of different length L .

L	Cubic phase gates	r_{max}	Beam splitters	Fourier gates	Worst-case Fidelity
6	4×18	0.069	4×18	$4 \times 6 + 6$	0.806
7	4×21	0.062	4×21	$4 \times 6 + 6$	0.901
9	4×27	0.052	4×27	$4 \times 8 + 6$	0.980
11	4×33	0.044	4×33	$4 \times 10 + 6$	0.993
13	4×39	0.039	4×39	$4 \times 12 + 6$	0.997
15	4×45	0.035	4×45	$4 \times 14 + 6$	0.998

cubic phase gates is available, this approximation could supersede the probabilistic controlled-NOT gates and allow for deterministic and universal quantum computing using photonic qubits. Moreover, Eq. (32) can, with little to no modification, be used to implement a CV self-Kerr as well as cross-Kerr gate when acting on CV states beyond just single-photon states like in the above scheme. While not further investigated in this paper, both have a wide array of applications.

For instance, a unit-fidelity, non-Clifford gate on physical GKP qubits is possible with a self-Kerr-based interaction $\sim \hat{n}^2$ [33]. The CZ gate as discussed in this section could also be realized near-deterministically based on a cross-Kerr-interaction number-QND approach including feedforward [84], though the single-mode model for treating the naturally available nonlinear optical interactions in this case must be handled with care [85]. Compared with other schemes that aim at obtaining quartic Kerr-type interactions and either employ large numbers of elementary cubic or quartic gates, starting in the thousands for similar fidelities [9, 38, 86], or a smaller number of then absolutely necessary quartic gates [70], our scheme only requires about a hundred elementary cubic single-mode gates. This is also distinct from the approach of Ref. [87] where a CV single-mode self-Kerr gate is obtained conditionally with Gaussian ancilla states and operations including homodyne measurements, assuming a two-mode controlled phase rotation gate is available, e.g., from Faraday interactions in atomic ensembles. Complementary to this, our paper demonstrates how to optically get the controlled phase rotation gate in the first place and then how to combine four such gates, instead of just a single one as in [87], to obtain CV Kerr gates in an unconditional and measurement-free fashion. Nonetheless, our decompositions for controlled phase rotation gates could also be applied to the scheme of Ref. [87].

Quantum error correction based on a system of sufficiently many physical, photonic qubits, for which the entangling gate discussed in this section works, would nevertheless come with a large experimental overhead. A more hardware-efficient, and hence potentially promising approach, makes use of bosonic quantum error correction

codes with physical oscillator states clearly beyond average photon numbers of one. An important candidate for this is the GKP code, which we treat next.

B. GKP state generation

In general, quantum error correction on a system of qubits typically comes with a large computational and hence experimental overhead. In this context, an interesting approach towards an optical fault-tolerant quantum computer employs “brighter” optical oscillator states rather than optical dual-rail qubits to encode the logical qubits. The probably most prominent of these encodings is the GKP code presented by Gottesman, Kitaev, and Preskill in 2001 [4], which already includes the possibility to correct errors that become manifest – and can be formally expanded – as small shifts in phase space. While experimental demonstrations of GKP-type states have been generally out of reach for many years and only happened very recently in the circuit-QED [88] and ion-trap [89] platforms, an optical, photonics-based realization of these highly non-Gaussian, nonclassical states appears very challenging [90], though some theoretical proposals exist (see, e.g., Refs. [30, 31, 91–93]), some of which depending on Kerr-type “elementary” or other quartic gates [91, 94, 95]. Our schemes are solely based upon single-mode cubic gates and passive linear optics, unlike, for instance, the recent proposal of Ref. [16] that requires suitable quantum optical multimode Hamiltonians of cubic order.

In this section, we give a brief overview of GKP states, codes, and gates, before we apply our optical gate decomposition method to a measurement-based [4] and a measurement-free [96] GKP state generation method. We shall also consider the creation of arbitrary logical GKP states including the so-called magic states.

1. GKP states, codes, and gates

The ideal GKP codewords are given by

$$|0_L\rangle = \sum_{s \in \mathbb{Z}} |x = ds\rangle, \quad |1_L\rangle = \sum_{s \in \mathbb{Z}} |x = d(s + \frac{1}{2})\rangle, \quad (37)$$

where $\langle x|x = x_0\rangle$ is the Dirac delta function $\delta(x - x_0)$ and $d \in \mathbb{R}$. They are unnormalizable and clearly unphysical states. However, they are orthogonal and can easily be distinguished by a homodyne measurement. Moreover, displacement errors in \hat{x} below a threshold of $\frac{d}{4}$ preserve the logical information. Using the Poisson summation formula we find that

$$|0_L\rangle = \sum_{s \in \mathbb{Z}} |p = \frac{2\pi}{d}s\rangle, \quad |1_L\rangle = \sum_{s \in \mathbb{Z}} (-1)^s |p = \frac{2\pi}{d}s\rangle, \quad (38)$$

with $\langle p|p = p_0\rangle = \delta(p - p_0)$. Therefore the same holds true for displacement errors in \hat{p} below a threshold of $\frac{\pi}{d}$. This

is remarkable, as an arbitrary error in a CV system can be expanded in terms of displacements,

$$\mathcal{E}(\hat{\rho}) = \int_{\mathbb{C}^2} d\beta d\beta' c(\beta, \beta') \hat{D}(\beta) \hat{\rho} \hat{D}^\dagger(\beta'), \quad (39)$$

with the displacement operator $\hat{D}(\alpha) = \exp(\alpha \hat{a}^\dagger - \alpha^* \hat{a})$ [4]. The ideal GKP code can thus correct any error with sufficiently small support of $c(\beta, \beta')$. Choosing $d = 2\sqrt{\pi}$ so that $\frac{\pi}{d} = \frac{d}{4}$ is referred to as square GKP code. The logical gates of the DV universal gate set of Eq. (3) for the square code are given by

$$\hat{H}_L = e^{i\frac{\pi}{2} \frac{\hat{x}^2 + \hat{p}^2}{2}}, \quad \hat{S}_L = e^{i\frac{\hat{x}^2}{2}}, \quad \text{CNOT}_L = e^{-i\hat{x}_1 \hat{p}_2}. \quad (40)$$

Moreover, the Pauli operators \hat{X}_L , \hat{Y}_L , and \hat{Z}_L can be straightforwardly realized using displacements, especially $\hat{X}_L = e^{-i\sqrt{\pi}\hat{p}}$ and $\hat{Z}_L = e^{i\sqrt{\pi}\hat{x}}$. The stabilizers of the code can then be written as \hat{X}_L^2 and \hat{Z}_L^2 . The syndrome measurements for displacement errors in \hat{x} and \hat{p} can be done subsequently by linearly coupling the GKP-encoded signal qubit with a suitable GKP ancilla qubit followed by corresponding homodyne detections. Notably, provided GKP states are available, all these operations are Gaussian and thus comparably easy to realize experimentally. This is one of the main advantages of the GKP code.

One gate from the DV universal gate set that still has not been considered yet is the non-Clifford gate \hat{T} . In the original proposal, it was suggested to employ the relation

$$\hat{T}_L = \exp\left(\frac{i\pi}{4} \left(2\left(\frac{\hat{x}}{\sqrt{\pi}}\right)^3 + \left(\frac{\hat{x}}{\sqrt{\pi}}\right)^2 - 2\left(\frac{\hat{x}}{\sqrt{\pi}}\right)\right)\right), \quad (41)$$

which holds true for the ideal GKP states. However, it was recently demonstrated that this operator is unsuitable for approximate finite-energy GKP states [32]. Instead, a “magic gate” can be obtained by “magic state injection”, a technique similar to gate teleportation using a logical magic state $|T_L\rangle = \frac{|0_L\rangle + e^{i\frac{\pi}{4}}|1_L\rangle}{\sqrt{2}}$ as off-line resource [7]. In general, it is possible to choose $d \neq 2\sqrt{\pi}$. For example, the so-called “qunaught state” $|q\rangle_{\text{GKP}}$ with $d = \sqrt{2\pi}$ fulfils $\hat{F}|q\rangle_{\text{GKP}} = |q\rangle_{\text{GKP}}$ and is useful when entangling two GKP states using a beam splitter to obtain a GKP Bell state [97]. Another common choice is the hexagonal GKP code with $d = 2(2\pi/\sqrt{3})^{\frac{1}{2}}$ and $\hat{H}_L = \hat{F}\left(\frac{\pi}{3}\right)$, which can correct arbitrary displacements below the threshold $(\frac{\pi}{2\sqrt{3}})^{\frac{1}{2}}$, related to the closest packing of circles in two dimensions. The Wigner functions of different GKP states are shown in Fig. 4.

The most common and practical approach to obtain physical approximations of the ideal GKP states is to replace the Dirac delta functions by Gaussian curves of width k^{-1} and introduce an overall Gaussian envelope of width k . Therefore, the resulting states

$$\langle x|0\rangle_{\text{GKP}}(k, d) \propto \sum_{s \in \mathbb{Z}} \exp\left(-\frac{(ds)^2}{2k^2} - \frac{k^2(x - ds)^2}{2}\right) \quad (42)$$

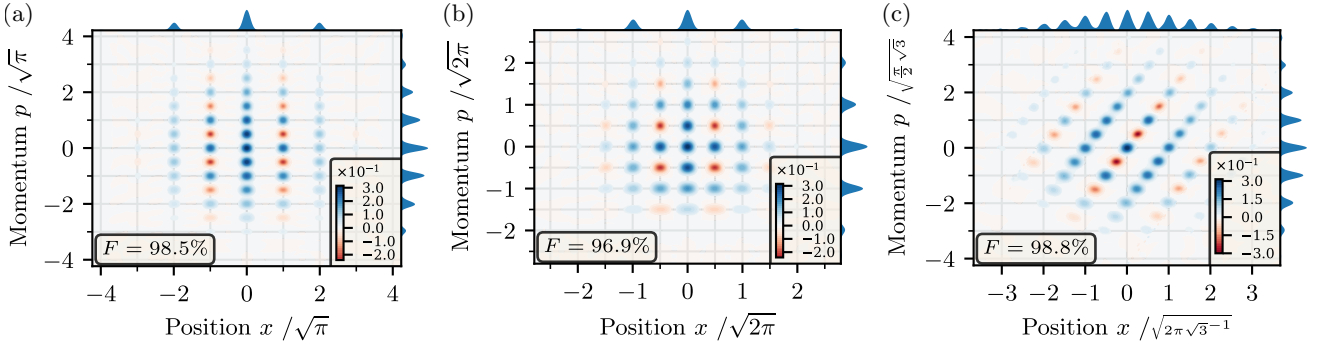


FIG. 4. Wigner functions of different approximated GKP states. (a) Approximated $|0\rangle_{\text{GKP}}$ state for $d = 2\sqrt{\pi}$, 12.2 dB squeezing ($n = 5$), and $L = 7$ cubic QND gates. (b) Approximated qunaught GKP state for $d = \sqrt{2\pi}$, 11.5 dB squeezing ($n = 2$), and $L = 9$ cubic QND gates. (c) Approximated hexagonal GKP state for $d = (2\pi\sqrt{3})^{1/2}$, 11.9 dB squeezing ($n = 4$), $L = 9$ cubic QND gates, $\delta = \frac{\pi}{2}$, and a -30° -phase rotation gate.

can be referred to as Gaussian GKP states, despite being highly non-Gaussian. In the case of high squeezing, where k is large, these Gaussian GKP states approach the ideal codewords and the probability to misidentify the two nonorthogonal states $|0\rangle_{\text{GKP}}$ and $|1\rangle_{\text{GKP}}$ becomes exponentially small,

$$P_{\text{Error}} < \frac{2}{\pi k} e^{-\frac{\pi}{4} k^2}. \quad (43)$$

Moreover, they fulfill the relation

$$|j\rangle_{\text{GKP}} \propto \int_{\mathbb{C}} d\alpha \exp(-|\alpha|^2 k^2) \hat{D}(\alpha) |j_L\rangle, \quad (44)$$

with $j = 0, 1$ [98]. Hence, the Gaussian GKP states can be regarded as ideal GKP states that have undergone a coherent displacement error of Gaussian distribution. This implies that the presented operators do approach their corresponding logical gates for large k , as Gaussian gates act only linearly on the operators \hat{x} and \hat{p} . At the same time, this illustrates why the nonlinear operation defined in Eq. (41) does not converge to the gate \hat{T}_L even for high squeezing.

The process of error correction also stays unchanged for approximate GKP states, as the code was designed to correct small displacements. Although the intrinsic error of the approximation reduces the margin of external errors that can be successfully corrected, simulations show that even for relatively low squeezing, the GKP code outperforms other CV error correction codes when considering photon loss as source of error [99].

2. GKP state generation with conditional measurement

While basic operations on the GKP code space as well as error correction are easily implementable in an optical context, the creation of high-quality optical GKP code-words still has not been accomplished 20 years after the original GKP proposal [100]. However, a creation scheme

as old as the code itself can also be found in the original Ref. [4]: Let a controlled phase rotation gate act upon a squeezed vacuum together with a “meter” and then measure the meter’s phase. More recently, in Ref. [101], this idea was revisited with a focus on an implementation in the circuit-QED platform. We shall discuss this particular concept for GKP state generation in a little more detail.

Here, we intend to propose a slightly altered version, tailored to work in a purely optical setting, based on the presented decompositions. First, we start with a squeezed vacuum together with a displaced state as a meter. Second, we replace the controlled phase rotation gate with our approximation to obtain

$$|\psi_{k,\alpha}(t)\rangle := S_{\lambda}(t) \left(e^{-i\frac{\ln(k)}{2}(\hat{x}\hat{p} + \hat{p}\hat{x})} |\text{vac}\rangle \right)_1 (e^{-i\alpha\hat{p}} |\text{vac}\rangle)_2. \quad (45)$$

Third, instead of phase estimation [101], we use a simple homodyne measurement in the quadrature \hat{p}_2 whilst conditioning the measurement result to $p_0 \approx 0$. In the ideal case of an infinite displacement and exactly $p_0 = 0$, this measurement will then fix the strength of the performed controlled phase rotation to multiples of π resulting in periodic peaks in the position wave function of mode 1 with a Gaussian envelope given by its initial squeezing. The case of a finite displacement and general measurement outcomes p_0 can also be treated analytically. Regarding the equations

$$0 = S_{\lambda}(t)(\sqrt{2}\hat{a}_2 - \alpha)S_{\lambda}(-t)|\psi_{k,\alpha}(t)\rangle, \quad (46)$$

$$0 = S_{\lambda}(t)(k^{-2}\hat{x}_1 + i\hat{p}_1)S_{\lambda}(-t)|\psi_{k,\alpha}(t)\rangle \quad (47)$$

in momentum and position space, replacing \hat{x}_1 with $i\partial_{p_1}$ and \hat{p}_2 with $-i\partial_{x_2}$, respectively, gives us two differential

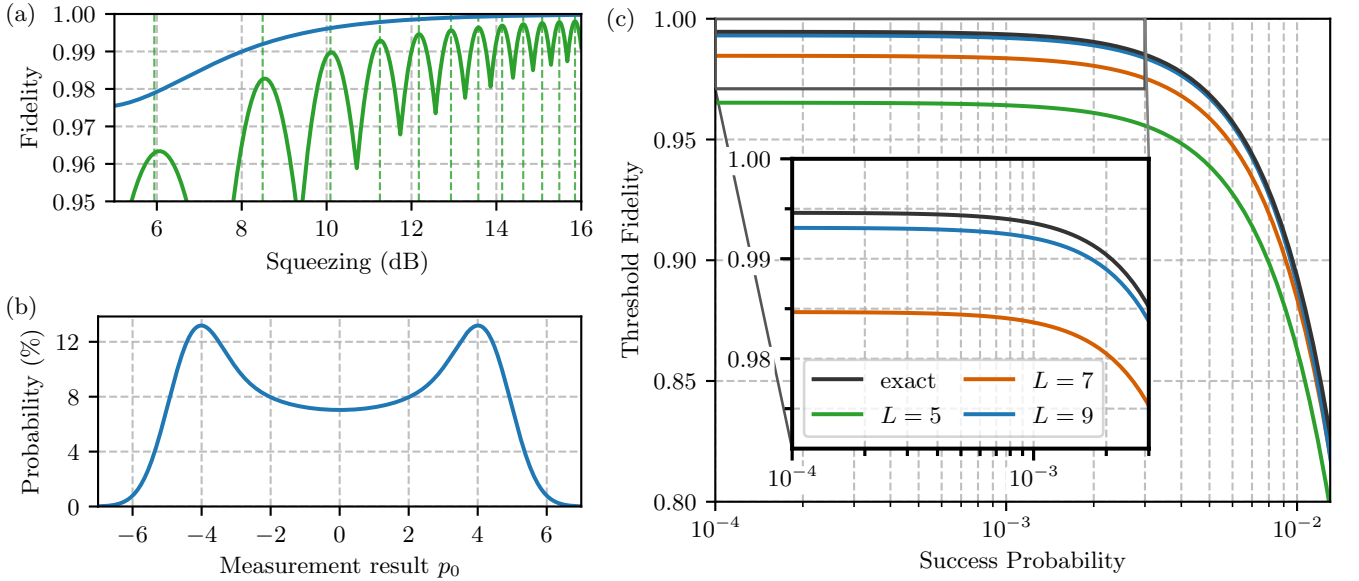


FIG. 5. Performance of the approximation for $d = 2\sqrt{\pi}$. (a) Fidelity to the target state $|0\rangle_{\text{GKP}}$ of the absolute value (blue) and after the phase correction (green) given $p_0 = 0$. The vertical green lines indicate the different n 's of Eq. (54). (b) Probability distribution of the homodyne measurement for a squeezing of 12.2 dB ($n = 5$). (c) Threshold fidelity against the success probability for different p_0 -conditionings $|p_0| \leq \text{const.}$ for a squeezing of 12.2 dB ($n = 5$) and different approximations to the controlled phase rotation gate. L represents the number of cubic QND gates used.

equations with the normalized solution

$$\langle x_1, p_0 | \psi_{k,\alpha}(t) \rangle = \frac{N}{\sqrt{A}} \exp\left(\frac{-x_1^2}{2k^2} - \frac{B}{2A} p_0^2 - i\frac{\alpha}{A} p_0\right) \times \exp\left(\frac{\alpha^2 P_{xx}[tx_1]}{2A}\right), \quad (48)$$

$$N = \frac{1}{\sqrt{\pi k}} \exp\left(i\varphi - \frac{\alpha_R^2}{2}\right), \quad (49)$$

with $A = P_{xx}[tx_1] + iP_{px}[tx_1]$, $B = P_{pp}[tx_1] - iP_{xp}[tx_1]$, the real part α_R and a global phase φ . Here the notation \sqrt{A} is used for the solution to the differential equation

$$\frac{f'(x)}{f(x)} = \frac{1}{2} \frac{A'(x)}{A(x)}. \quad (50)$$

The imaginary phase of the function $\sqrt{A}(x)$ thus covers the full range of $(-\pi, \pi]$ instead of the common $(-\frac{\pi}{2}, \frac{\pi}{2}]$.

Before we look at the approximation's impact on the scheme, let us consider the case of an ideal controlled phase rotation gate. Replacing the polynomials with sine and cosine, respectively, we get

$$\langle x_1, p_0 | \psi_{k,\alpha}(t) \rangle \propto \exp\left(-\frac{x_1^2}{2k^2} - \frac{|\alpha|^2}{2} \sin^2(tx_1 + \delta)\right) \times \exp\left(i\frac{tx_1}{2} + i\frac{|\alpha|^2}{4} \sin(2tx_1 + 2\delta)\right) \times \exp(-ip_0 |\alpha| \exp(itx_1 + i\delta)), \quad (51)$$

with $\alpha = |\alpha| e^{i\delta}$. In order to obtain the correct spacing and squeezing of the GKP code, we must have $t = \pi/d$

and $|\alpha| = k/t$. The initial phase of the displaced state δ provides an elegant way of shifting the peaks, while keeping the Gaussian envelope centered. For the state $|0\rangle_{\text{GKP}}$, however, we will be setting it to $\delta = 0$.

With these parameters set, let us look at the terms of Eq. (51) line by line. The first line gives the absolute value of the waveform and approximates $\langle x|0\rangle_{\text{GKP}}$ quite well for $k \gg 1$, since

$$\exp\left(-\frac{k^2 d^2}{2\pi^2} \sin^2\left(\frac{\pi x}{d}\right)\right) \stackrel{k \gg 1}{\approx} \sum_{s \in \mathbb{Z}} \exp\left(-\frac{k^2 (x - ds)^2}{2}\right). \quad (52)$$

The second line gives the phase of the waveform. On the one hand, the first term is due to the negligence of the $-\frac{1}{2}$ term in $\hat{n} = \hat{x}^2 + \hat{p}^2 - \frac{1}{2}$ and easily corrected by introducing a corrective displacement of $t/2$. On the other hand, the second term arises from the homodyne measurement and needs a bit more attention. As it takes the same form for every peak, it is sufficient to regard its impact on the fidelity of two single Gaussians,

$$\begin{aligned} & \left| \int e^{-k^2 \varepsilon^2} \exp\left(i\frac{k^2 d^2}{4\pi^2} \sin\left(\frac{2\pi \varepsilon}{d}\right) - i\varepsilon \cdot c\right) d\varepsilon \right| \\ & \approx \int e^{-\varepsilon^2} \cos\left(\frac{c'}{k} \varepsilon - \frac{\pi}{3kd} \varepsilon^3 + \mathcal{O}\left(\frac{1}{k^3}\right)\right) \frac{d\varepsilon}{k} \\ & = \int e^{-\varepsilon^2} \left(-\frac{c'^2 \varepsilon^2}{k^2} + \frac{c'}{k^2} \frac{\pi \varepsilon^4}{3d} + \mathcal{O}\left(\frac{1}{k^4}\right)\right) \frac{d\varepsilon}{k} + \text{const.} \\ & = \frac{\sqrt{\pi}}{k^3} \left(-\frac{c'^2}{4} + c' \frac{\pi}{4d} + \mathcal{O}\left(\frac{1}{k^2}\right)\right) + \text{const.}, \end{aligned} \quad (53)$$

TABLE III. List of resources needed for the different presented GKP state generation schemes. The maximal required cubic phase gate strength of each scheme is denoted by r_{max} .

Figure	Target state	Fidelity	Squeezing [dB]	Cubic phase gates	r_{max}	Beam splitters	Fourier gates	Displacements	Other
2	$ 0\rangle_{\text{GKP}}$	0.909	12.2	7	0.130	9	2	2	
4 (a)	$ 0\rangle_{\text{GKP}}$	0.985	12.2	15	0.068	21	6	2	
4 (b)	$ q\rangle_{\text{GKP}}$	0.969	11.5	19	0.066	27	8	2	
4 (c)	hex. $ 0\rangle_{\text{GKP}}$	0.988	11.9	19	0.100	27	8	2	$e^{-i\frac{\pi}{6}\hat{n}}$
6 (b)	$ T\rangle_{\text{GKP}}$	0.927	12.0	33	0.036	48	16	2	
7	$ 1\rangle_{\text{GKP}}$	0.972	11.5	$4 \times 10 \times 24$	0.061	$4 \times 10 \times 54$	$4 \times 10 \times 12 + 8$		$ 0\rangle_{\text{DR}}$
9	$ T\rangle_{\text{GKP}}$	0.991	11.7	$19 + 2 \times 44$	0.153	$27 + 2 \times 99$	$8 + 2 \times 22 + 4$	3	$ T\rangle_{\text{DR}}$

with an additional displacement c and $c' = -c + k^2/2t$. Consequently, given $k \gg 1$, the approximation is best for $c = k^2/2t - t/2$ and a total corrective displacement of $k^2/2t$. On the other hand, in order to take the same form for every peak, the additional displacement must fulfill $c = 2t \cdot n$ with $n \in \mathbb{Z}$. This leads us to the following condition for the optimal squeezing parameter:

$$k = 2t\sqrt{n + 1/4}, \quad n \in \mathbb{Z}. \quad (54)$$

When states with different spacing t but identical squeezing k are needed, it is useful to choose a squeezing parameter for which both states show minimal deviation from the optima, for example $2\sqrt{n + 1/4 + 1/20} = \sqrt{n' + 1/4 - 1/20}$. The performance of this phase correction compared to that of the absolute value can be seen in Fig. 5(a). A change of the fixed peak spacing d whilst keeping n constant is found to have a negligible effect on the calculated fidelities.

The third line gives the error introduced by a measurement result of $p_0 \neq 0$. Although this term will later prove useful in the creation a GKP magic state, here it is nothing but an uncorrectable but preventable error. Accepting a larger interval of measurement results p_0 increases the maximum error, while a smaller acceptance interval lowers the success probability. The introduced errors and success probabilities for a squeezing of 12.2 dB ($n = 5$) can be found in Fig. 5(c). Larger n , whilst leading to an increased maximum fidelity, are found to be accompanied by smaller success probabilities.

Up to now we have not considered the impact of an approximated controlled phase rotation gate yet. In order to do so, we optimize parameter sets λ of different length L to maximize the fidelity of the approximation and its target state for $p_0 = 0$. The results are plotted in Fig. 5(c). They show that it is possible to achieve a practically perfect approximation to the controlled phase rotation gate with less than ten as well as fidelities over 96% with merely five cubic QND gates. As a general rule, the more peaks the target state has, the more gates are needed to approximate it properly. Hence, states such as $+$, $-$, quanaught, and hexagonal GKP states tend to need a higher squeezing as well as a higher operator count to

achieve the same fidelities as the $|0\rangle_{\text{GKP}}$ state. The parameters needed to obtain the different GKP states and encodings are summarized in Table IV, while the resulting Wigner functions of the GKP states considered here, given similar squeezing and operator counts, are shown in Fig. 4.

Note that all these GKP states can be created using $2L + 1$ cubic phase gates of the same gate strength. This is demonstrated in the exemplary circuit of Fig. 2 and is likely to be significant for their experimental feasibility. In fact, a recent experimental demonstration [8] would correspond to a cubic-phase-gate strength parameter r in Eq. (9) as $r \approx 0.17$. In Appendix B we present optimized parameter sets for the scheme of Fig. 2 where we can choose all gate strengths identical and below a value of 0.17. Weaker gate strengths may allow to improve the final state fidelities for larger gate concatenations. When sticking to the scheme of Fig. 2 the optimized non-identical gate strengths include a maximal value of 0.13 (see Appendix B). For an easy comparison the amount of elementary gates as well as the maximal cubic-phase-gate strength r_{max} needed to generate the different GKP states are also summarized in Table III.

3. Creating a GKP magic state

Besides creating the logical GKP codewords, there is one more obstacle to overcome in order to achieve full universality with optical GKP qubits: a qubit non-Clifford gate such as \hat{T} that acts logically in the corresponding way when applied upon GKP states, like \hat{T}_L of Eq. (41) as originally proposed in Ref. [4] and discussed in Secs. II A and IV B 1. The original approach though performs rather poorly on finitely squeezed states [32] and an optimized version was found to saturate at a logical fidelity of about 95% for high squeezing [7]. The more promising approach is therefore the gate teleportation of a magic state $|0\rangle_{\text{GKP}} + e^{i\frac{\pi}{4}}|1\rangle_{\text{GKP}}$ [4, 7], as was also mentioned before. Here we want to discuss how our optical GKP creation scheme can be used to approximate a GKP magic state. The underlying idea is to change the

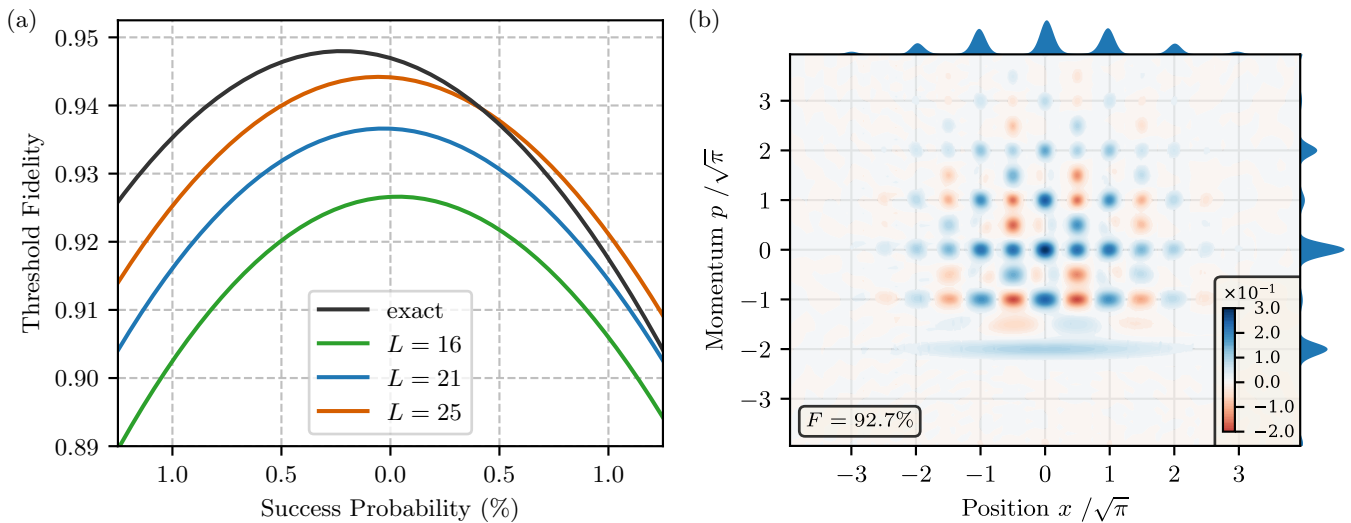


FIG. 6. Approximating a GKP magic state. (a) Fidelity to the target state $|T\rangle_{\text{GKP}}$ plotted against the success probability for a squeezing of 12.0 dB ($n = 1$) and different approximations to the controlled phase rotation gate. L represents the number of cubic QND gates employed. As the fidelity is not symmetric around $p_0 = \frac{\pi^2}{8kd}$, success is defined one-sided: $\text{const.} \leq p_0 \leq \frac{\pi^2}{8kd}$ to the left and $\frac{\pi^2}{8kd} \leq p_0 \leq \text{const.}$ to the right. (b) Approximated $|T\rangle_{\text{GKP}}$ state using $d = \sqrt{\pi}$, $p_0 = \frac{\pi^2}{8kd}$, 12.0 dB squeezing ($n = 1$) and $L = 16$.

TABLE IV. Parameters used to approximate GKP states of different encodings.

Encoding	State	t	p_0	δ
Square	$ 0\rangle_{\text{GKP}}$	$\sqrt{\pi}/2$	0	0
Square	$ 1\rangle_{\text{GKP}}$	$\sqrt{\pi}/2$	0	$\frac{\pi}{2}$
Qunaught	$ q\rangle_{\text{GKP}}$	$\sqrt{\pi}/2$	0	0
Hexagonal	$ 0\rangle_{\text{GKP}}$	$(\pi/(2\sqrt{3}))^{1/2}$	0	$\frac{\pi}{2}$
Square	$ T\rangle_{\text{GKP}}$	$\sqrt{\pi}$	$\frac{\pi}{8 \alpha }$	0

p_0 conditioning and make use of the introduced error.

Let us take a look at the p_0 dependence of Eq. (51),

$$\exp\left(-ip_0 \frac{kd}{\pi} \exp(itx_1)\right). \quad (55)$$

Accepting the measurement result only when $p_0 \approx \frac{\pi^2}{8kd}$ we obtain a phase of

$$\exp\left(i \frac{\pi}{4} \frac{1 - \cos(tx_1)}{2}\right), \quad (56)$$

up to a global phase. This is a fairly good approximation of a logical \hat{T} gate in the sense that every second GKP peak obtains a phase of $e^{i\frac{\pi}{4}}$. This means, however, that in order to get a magic state, we need to start with a peak spacing of $d = \sqrt{\pi}$ provided with a $|+\rangle_{\text{GKP}}$ state. When using the same squeezing as for the $|0\rangle_{\text{GKP}}$ state, this implies that the fidelity of the magic state will be inherently worse. The resulting fidelity saturates at 94.8% for a comparable squeezing of 12.0 dB ($n = 1$) independent of the operator count L , but with a higher success

probability (see Fig. 6). In order to obtain higher fidelities, a higher squeezing must be chosen, for example, a squeezing of 14.5 dB ($n = 2$) allows for fidelities up to 97.7%. It might also be possible to use the more accurate logical GKP states in order to distil magic states of higher fidelity. On the other hand, the scheme presented in the next section can be used to create a magic state from a high-fidelity $|0\rangle_{\text{GKP}}$ state. Let us finally mention that when using $|+\rangle_{\text{GKP}}$ states to initiate the logical qubits, logical qubits and magic states could be generated in parallel given a two-part acceptance interval for the measurement outcomes.

4. Measurement-free GKP state generation

One of the main advantages of a purely optical quantum computer is the achievable clock rate. Therefore it would be desirable to have a deterministic, measurement-free scheme as opposed to the probabilistic GKP state creation of the preceding sections. In Ref. [96], the authors present a measurement-free GKP creation scheme using the Rabi-type Hamiltonian gates $e^{i\hat{p}\hat{\sigma}_x}$ and $e^{i\hat{x}\hat{\sigma}_y}$, which are readily available in trapped-ion and superconducting circuit platforms, where the spin operators can either act upon a real or an “artificial” two-level atom. In fact, there are already experimental demonstrations in these platforms based on similar concepts [102, 103]. Here, however, we shall apply our decomposition results for purely optical Rabi-type Hamiltonians of Sec. III C to the GKP state generation scheme of Ref. [96].

Using the gates $U_k = e^{iu_k \hat{x} \hat{\sigma}_y}$, $V_k = e^{iv_k \hat{p} \hat{\sigma}_x}$, and $W_k = e^{iw_k \hat{x} \hat{\sigma}_y}$ and applying them on an infinitely squeezed state

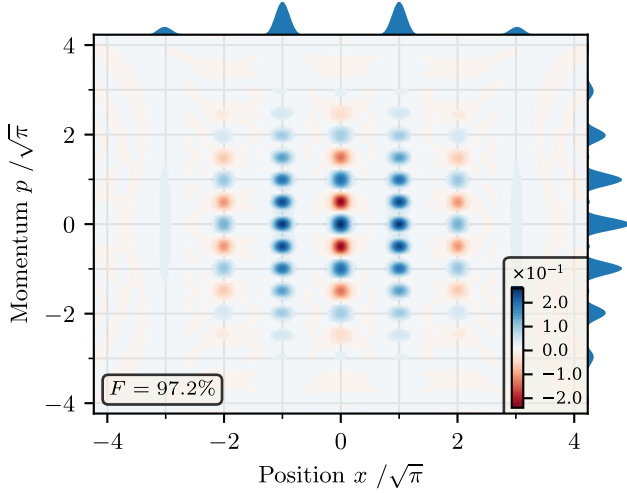


FIG. 7. Approximating a $|1\rangle_{\text{GKP}}$ state using the measurement-free protocol of Ref. [96] with $N = 2$, a squeezing of 11.5 dB, $u_2 = 0.093$, and $L = 60$ CV Toffoli gates for each of the four approximated Rabi-type Hamiltonians.

$|x_0\rangle$ and a qubit ancilla state $\alpha|+\rangle_a + \beta|-\rangle_a$ as an input, one obtains

$$\begin{aligned}
& W_k V_k U_k |x_0\rangle (\alpha|+\rangle_a + \beta|-\rangle_a) \\
&= W_k V_k |x_0\rangle (A|+\rangle_a + B|-\rangle_a) \\
&= W_k (A|x_0 - v_k\rangle|+\rangle_a + B|x_0 + v_k\rangle|-\rangle_a) \\
&= \cos(w_k x_0) (A|x_0 - v_k\rangle \mp B|x_0 + v_k\rangle) \begin{cases} |1\rangle_a \\ |0\rangle_a \end{cases} \\
&+ \sin(w_k x_0) (\pm A|x_0 - v_k\rangle - B|x_0 + v_k\rangle) \begin{cases} |0\rangle_a, \text{ if } v_k w_k = +\frac{\pi}{4} \\ |1\rangle_a, \text{ if } v_k w_k = -\frac{\pi}{4} \end{cases}
\end{aligned} \tag{57}$$

with

$$A = \alpha \cos(u_k x_0) - \beta \sin(u_k x_0), \tag{58}$$

$$B = \beta \cos(u_k x_0) + \alpha \sin(u_k x_0). \tag{59}$$

As we can see, the displacement gate V_k displaces $|x_0\rangle$ depending on the state of the qubit, effectively splitting it in two. The disentangling gate W_k then disentangles qubit and qumode again if and only if $v_k w_k = \pm \frac{\pi}{4}$ and $w_k x_0 = m \cdot \frac{\pi}{2}$ with $m \in \mathbb{Z}$. The preparation gate U_k , on the other hand, rotates the ancilla qubit depending on the position x_0 and together with the original qubit state determines the amplitudes of the two resulting squeezed states $|x_0 - v_k\rangle$ and $|x_0 + v_k\rangle$.

When repeating this procedure N times it is thus possible to split the original $|x_0\rangle$ state into a sum of 2^N distinct position states. Starting with $|x_0 = 0\rangle|0\rangle_a$ and choosing the v_k and w_k to be

$$v_k = \begin{cases} -\sqrt{\pi} 2^{N-1}, & \text{if } k = 1, \\ +\sqrt{\pi} 2^{N-k}, & \text{if } k > 1, \end{cases} \tag{60}$$

$$w_k = \begin{cases} -\frac{\sqrt{\pi}}{4} 2^{-(N-k)}, & \text{if } k < N, \\ +\frac{\sqrt{\pi}}{4}, & \text{if } k = N, \end{cases} \tag{61}$$

we obtain the state

$$\left(\sum_{k=1}^{2^N} c_k |(2k-1-2^N)\sqrt{\pi}\rangle \right) |0\rangle_a \approx |1\rangle_{\text{GKP}} |0\rangle_a. \tag{62}$$

The weights of the different peaks c_k are determined by the strengths of the preparation gates u_k . Different sets of the latter optimized for different figures of merit can be found in Ref. [96]. Note that generally setting $u_1 = 0$ and combining the operators W_k and U_{k+1} reduces the number of required Hamiltonians to $2N$. When introducing finitely squeezed states as an input, the preparation and disentangling gates are no longer exact. After tracing out the qubit ancilla, this leads to a mixed final state. Measuring the ancilla qubit after each iteration could therefore provide pure final states together with overall higher fidelities. However, this is not necessary, as the measurement-free scheme on its own is already able to produce high-fidelity states for simply $N \geq 2$.

Replacing the Rabi-type Hamiltonian gates with the presented approximations using the $T_\lambda(t)$ gate on an optical qumode together with an optical dual-rail qubit, we are able to translate this protocol into a purely optical setting. The resulting $|1\rangle_{\text{GKP}}$ state for $N = 2$, a squeezing of 11.5 dB, $u_2 = 0.093$, and $L = 60$ CV Toffoli gates for each of the four approximated Hamiltonians can be seen in Fig. 7. The results show that it is possible to deterministically create GKP states using only single-mode cubic phase gates, beam splitters, phase rotations, and off-line squeezing together with an off-line single-photon qubit ancilla state.

However, the number of gates needed to properly approximate this protocol is significantly higher than for the probabilistic one. This can be attributed to two factors. On the one hand, due to an already computationally expensive fidelity calculation, in this case we refrained from doing a parameter optimization and instead used the third-order set $\lambda = (0.397, -0.794, -0.0325, 1.54, 0.636, 0.254)^T$, which had proven effective in previous applications. On the other hand, the relatively high gate strength $v_1 = 2\sqrt{\pi}$, corresponding to a $d = \frac{\sqrt{\pi}}{2}$ in the probabilistic scheme, is generally harder to approximate, as this increases the number of relevant sine/cosine periods.

5. Creating arbitrary logical GKP states

Another useful application of the above protocol is the creation of arbitrary logical states. While simple changes in the parameters u_k , v_k , and w_k are sufficient to obtain states of nonsquare encodings such as rectangular and hexagonal $|1\rangle_{\text{GKP}}$ states [96], modifying the initial state of the ancilla qubit enables us to create arbitrary logical states. Choosing $u_1 = 0$, $v_1 = -\frac{\sqrt{\pi}}{2}$, and $w_1 = \frac{\sqrt{\pi}}{2}$ together with an additional displacement and a $|0\rangle_{\text{GKP}}$ state as an

input, we have

$$\begin{aligned} & \exp\left(i\frac{\sqrt{\pi}}{2}\hat{p}\right)W_1V_1U_1\left(\sum_{k\in\mathbb{Z}}c_k|2k\sqrt{\pi}\right)(\alpha|+\rangle_a+\beta|-\rangle_a) \\ &= \sum_{k\in\mathbb{Z}}c_k(-1)^k(\alpha|2k\sqrt{\pi}\rangle+\beta|(2k-1)\sqrt{\pi}\rangle)|0\rangle_a. \end{aligned} \quad (63)$$

Alternatively, the same result can be obtained for a $|1\rangle_{\text{GKP}}$ state as an input by straightforward modifications to the parameters.

Two aspects of the final state still need to be addressed. First, the term $(-1)^k$ is clearly unwanted and in the original proposal of Ref. [96], it gets corrected by a displacement in p . This, however, introduces linear error terms. Another option is to run the protocol twice using a $|+\rangle$ ancilla on the first and an ancilla in the sought after logical state on the second run. Moreover, both GKP creation schemes presented in this paper can naturally compensate for this term: in the probabilistic scheme this is done by choosing $n = n_0 + \frac{1}{2}$ with $n_0 \in \mathbb{N}$, while in the deterministic protocol it is sufficient to invert the sign of w_N . Second, shaping the overall form of the peaks using U_1 mixes the coefficients α and β , and is thus problematic for some aspired states. Moreover, while using a $|0\rangle_{\text{GKP}}$ state displaced by $\sqrt{\pi}$ as $|1\rangle_{\text{GKP}}$ state has a negligible effect on the fault tolerance of the code, it heavily influences the calculated fidelities (as much as 10% for a squeezing of 11.5 dB). In order to not distort the results, the fidelities are therefore calculated towards the target state $\alpha|0\rangle_{\text{GKP}} + \beta\exp(i\sqrt{\pi}\hat{p})|0\rangle_{\text{GKP}}$ instead of the usual $\alpha|0\rangle_{\text{GKP}} + \beta|1\rangle_{\text{GKP}}$.

In order to test the protocol we are again going to look at the creation of a GKP magic state. Not yet considering the gate approximations, its core performance for different squeezing levels when choosing $\alpha = 1/\sqrt{2}$ and $\beta = (1+i)/2$ is plotted in Fig. 8. The results show that when tracing over the qubit ancilla the fidelity of the resulting mixed state is highly dependent on the squeezing level of the input. Measuring the qubit ancilla, on the other hand, gives a pure state with significantly increased fidelity.

Incorporating the gate approximations of the optical setting, the operators of Eq. (63) can be rewritten as

$$\exp\left(i\frac{\sqrt{\pi}}{2}\hat{p}\right)\hat{F}_3T_\lambda\left(\frac{\sqrt{\pi}}{2}\right)\hat{F}_3^\dagger\hat{F}_1^\dagger T_\lambda\left(\frac{\sqrt{\pi}}{2}\right)\hat{F}_1. \quad (64)$$

Consequently, creating a GKP magic state from a given $|0\rangle_{\text{GKP}}$ state enables the repeated use of the same approximated Rabi-type Hamiltonian gate $T_\lambda(t)$ and, as its gate strength is comparably low, allows to approximate the results of Fig. 8 well using no more than 10 CV Toffoli gates. This is in stark contrast to the creation of a $|1\rangle_{\text{GKP}}$ state from scratch using the same protocol. It is therefore close at hand to combine the probabilistic creation of a high fidelity $|0\rangle_{\text{GKP}}$ state with Eq. (64). The resulting magic state after measuring the ancilla qubit can be seen in Fig. 9. This shows that it is possible

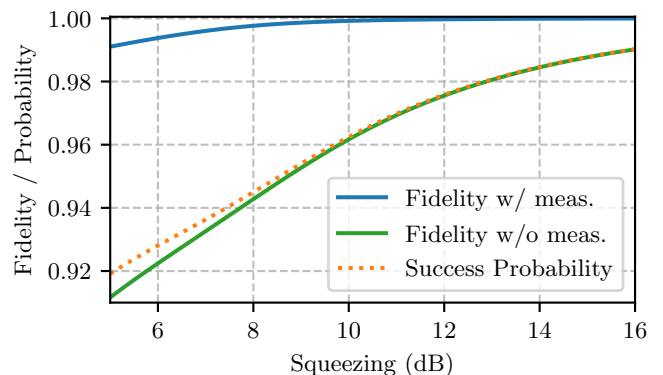


FIG. 8. Performance of the protocol of Eq. (63) applied on a Gaussian $|0\rangle_{\text{GKP}}$ state as in Eq. (42) with alternately signed peaks and varying squeezing as an input. The green line gives the fidelity to the magic state $\frac{1}{\sqrt{2}}|0\rangle_{\text{GKP}} + \frac{(1+i)}{2}e^{i\sqrt{\pi}\hat{p}}|0\rangle_{\text{GKP}}$ after tracing over the ancilla qubit. The blue and orange dotted lines, respectively, show the fidelity and success probability when measuring the ancilla qubit.

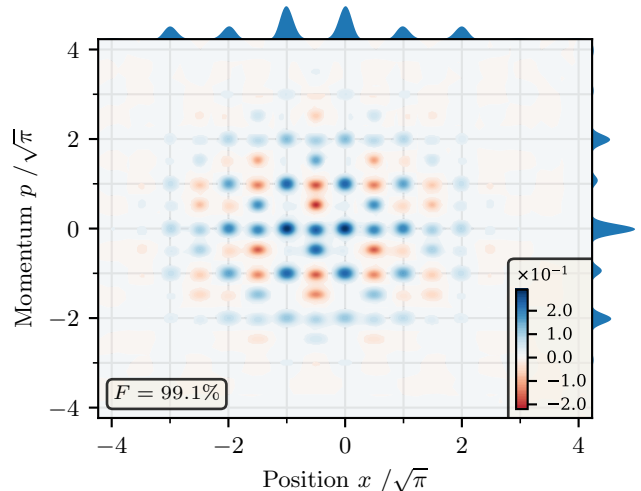


FIG. 9. Approximating a GKP magic state using a combination of the two presented creation methods. First, a $|0\rangle_{\text{GKP}}$ state with alternately signed peaks is created using the probabilistic scheme with $d = 2\sqrt{\pi}$, 11.7 dB squeezing ($n = 4.5$), and $L_1 = 9$ cubic QND gates. Then the protocol of Eq. (63) with $\alpha = 1/\sqrt{2}$ and $\beta = (1+i)/2$ is approximated using $L_2 = 11$ CV Toffoli gates for the two Rabi-type Hamiltonians. Finally, the dual-rail qubit is measured with a success probability of 93.7%. Without the measurement the same procedure gives a mixed state with a fidelity of 95.3%.

to obtain high-fidelity GKP magic states even for relatively low squeezing and a reasonable number of cubic QND as well as CV Toffoli gates. At the same time, it emphasizes the notion that, as opposed to the probabilistic schemes, the deterministic creation of arbitrary logical GKP states, whilst possible, still comes with high requirements on the amount of experimental resources.

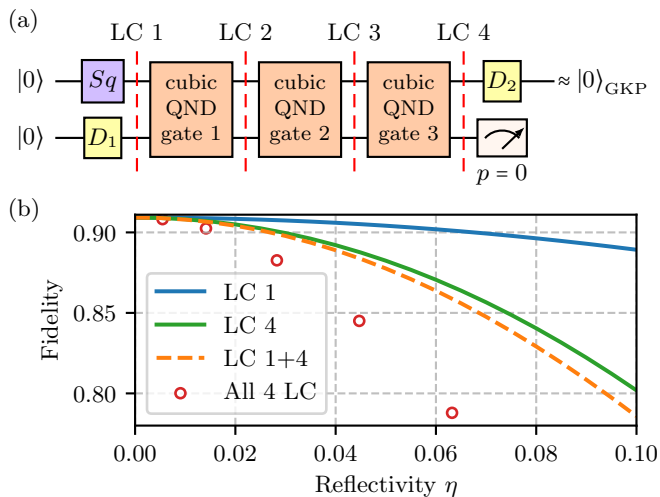


FIG. 10. Effects of photon loss on the circuit of Fig. 2. (a) Positioning of the different photon-loss channels. Each channel consists of two loss beam splitters with a reflectivity of η , one per mode. (b) Impact on the fidelity of the approximated GKP state for different sets of active photon-loss channels.

V. EXPERIMENTAL IMPERFECTIONS: PHOTON LOSS

Let us now consider the effect of experimental errors on the presented approximations. In a purely optical setup, these are primarily comprised of photon loss as well as imperfect gates from the universal gate set. As an exhaustive analysis of these errors and their impact on the different schemes goes beyond the scope of this paper, we are going to focus on one exemplary case: the effect of photon loss on the circuit of Fig. 2.

Photon loss can be modelled by introducing a beam splitter $\hat{B}_{1a}(s)$ with the reflectivity $\eta \equiv \sin(s) \ll 1$, which reflects a part of the given light mode out into a second mode $|\text{vac}\rangle_a$ representing the environment. Two of these loss beam splitters are then needed to cover the two modes of the circuit. For simplicity as well as computability, we will not consider losses happening within the cubic QND gates, leaving us with four places in the circuit where the beam splitters can be positioned, namely after each of the three cubic QND gates as well as after the squeezed and displaced input states. This is shown in Fig. 10(a). The impact of these eight loss beam splitters on the fidelity of the resulting GKP state in dependence of the reflectivity η can be seen in Fig. 10(b). Besides including all these eight loss beam splitters, the effect of faulty input states and a single erroneous cubic QND gate on their own is also shown. On the one hand, we find that errors of the input states impact the resulting GKP state less than errors occurring later on in the circuit. On the other hand, even for photon loss taking place throughout the scheme the fidelity of the final state still converges to its no-loss value surpassing 90% for $\eta < 0.015$. Note that the reflectivity parameter that represents the

effect of photon loss in our model describes the fraction of the signal mode operator's amplitude, which is subtracted from the signal. The more standard photon loss probability would then be η^2 , corresponding to a photon transmission of $1 - \eta^2$.

Another observation is that the impact of multiple errors is less than the sum of their individual impacts. Thus several small errors are less harmful than one large one. To which degree these findings hold for other sources of error and the different applications remains untested. It is crucial that the circuits that we derived for various applications are sufficiently short, i.e., contain only a small number of CV cubic gates, unlike previous decomposition schemes that rely upon commutator approximations [9, 38] or also higher nonlinear, namely quartic elementary CV gates [70, 86]. In particular, the GKP state generations are not fault tolerant, since the initial quantum optical resource states are not protected against lossy or even faulty CV gates by a quantum error correction code – the encoded, protected GKP state will only be the result of the application of the CV gate sequences. Nonetheless, the tolerable loss rates that we obtained above are comparable with the values proposed in other schemes and error or loss rates of the order 10^{-3} or 10^{-4} per gate are not an uncommon requirement of fault-tolerant schemes that are already based on concatenated quantum error correction codes. These thresholds may be reduced, but the necessary codes may then be more complicated, which would in turn have a negative impact on potential experiments.

Note that for some of the other applications that are possible with our decompositions, loss or fault tolerance can be provided. An example for this would be a non-Clifford gate on GKP qubits that approaches unit fidelity with high-quality GKP states based on a self-Kerr interaction $\sim \hat{n}^2$ [33]. In this case, the states are protected to some extent against the effect of physical CV error channels, also when sequences of CV gates are applied, provided the GKP states are of sufficient quality [47, 48, 104]. Nevertheless, also for this application, to combine fault tolerance with scalability, even when a time-domain approach is employed [1, 2], it is useful to minimize the length of the CV circuits. In previous schemes, decompositions for Kerr-type gates would be typically based on long gate sequences involving commutator approximations [9, 38, 86] or at least quartic elementary CV gates [70]. Generally, the results give confidence that the approximations presented in this paper can function even within the inherently noisy experimental setting, provided an appropriate threshold.

VI. CONCLUSIONS

In conclusion, we have demonstrated that a limited number of single-mode CV cubic phase gates – the canonical non-Gaussian gate of standard CV quantum computation – is a useful and sufficient resource for various ele-

ments in photonic quantum computation. This includes optical schemes for DV and CV quantum information processing. Unlike existing schemes that typically rely on complicated commutator approximations and hence require long CV gate sequences, our decomposition method is “hybrid”: it employs exact decompositions whilst possible and only reverts back to efficient approximations for mixing the x and p variables.

We have explicitly analyzed the performance of our method for three applications: (i) a two-qubit two-photon, entangling controlled- Z gate, (ii) a homodyne-measurement-based, conditional, optical GKP state generation scheme based on Gaussian resource states, and (iii) a measurement-free, optical GKP state generation scheme based on Gaussian and single-photon resource states. Our quantitative results imply that tens of single-mode cubic phase gates together with CV Fourier gates and beam splitters are sufficient to create high-fidelity GKP states, in the form of standard logical Pauli eigenstates or even “magic states”, and also to realize a deterministic, two-qubit two-photon controlled- Z gate in an optical setting. The GKP magic states can be employed to obtain a GKP qubit non-Clifford gate by means of gate teleportation techniques [7]. Another option would be to directly apply a quartic self-Kerr gate upon the GKP qubits, which, in principle, would allow for a unit-fidelity GKP non-Clifford gate operation [33]. We have demonstrated that our efficient decomposition method can be applied to such Kerr gates. Consequently, single-mode cubic phase gates are a suitable resource for all-optical, fault-tolerant, universal quantum computing.

More specifically, it was shown that the hybrid gate decomposition scheme consisting of exact decomposition techniques and efficient Trotterization is a powerful tool in creating non-Gaussian gates in an optical context. We were able to build a two-mode controlled phase rotation gate $e^{i\hat{x}_1\hat{n}_2}$ as well as the three Rabi-type Hamiltonians corresponding to the three-mode unitaries $e^{i\hat{x}_1\hat{\sigma}_x,s}$, $e^{i\hat{x}_1\hat{\sigma}_y,s}$, and $e^{i\hat{x}_1\hat{\sigma}_z,s}$ where the spin operators refer to the two-mode Schwinger representation. Testing their performance in different applications for photonic qubits, qumodes, as well as a mixture of both, it was shown that in most cases less than 30 single-mode cubic phase gates are already sufficient in providing a good approximation.

Regarding an optical creation of GKP states, this represents a significant improvement over previously known optical generation schemes based on the application of CV circuits that include nonlinear gates. Compared to a “Gaussian Boson Sampling” setup, our presented schemes do not reach the same fidelities to the target state but increase the success probability by multiple or-

ders. In order to synchronize the optical quantum states and make them available when needed – quasi on demand, the effect of the calculated success probabilities could be circumvented by the use of all-optical, cavity-based quantum memories [105]. These would even allow to optically store complicated, phase-sensitive, CV states such as GKP states [106].

The all-optical quantum memories experimentally demonstrated so far have “lifetimes” of the order of 100 ns. Thus, an event rate of 10^7 Hz would effectively lead to an on-demand source. Assuming a broadband source of especially Gaussian resource states, considering our conditional GKP state generation scheme, a 10 GHz repetition rate or equivalently 10^{10} pulses per second would be feasible. A success probability for the conditional state generation of the order of 10^{-3} would then result in a quasi-on-demand GKP qubit source. Our calculations suggest that GKP state fidelities around 0.995 are possible for such values of the success probability, though assuming an ideal, loss-free scheme. We also presented a short loss analysis, which implies demanding loss thresholds, but confirms the in-principle functioning of our scheme. In order to fully realize such a scheme, the elementary single-mode cubic phase gates could be incorporated quasi-on-demand by combining cubic phase gate teleportation techniques with all-optical quantum memories of ~ 100 ns lifetime.

Considering the advances of experimental single-mode cubic phase gates [8], it is hoped that these results may lead the way towards an experimental realization of optical GKP states as well as other applications. As all four relevant Hamiltonians of our schemes are experimentally available in trapped-ion and superconducting circuit platforms, there is a multitude of existing applications, which the presented approximations could help bring into the optical context. The scope of this hybrid gate decomposition scheme thus reaches far beyond the creation of optical GKP states or two-qubit two-photon entangling gates.

ACKNOWLEDGMENTS

We acknowledge funding from the BMBF in Germany (QR.X, PhotonQ, QuKuK, QuaPhySI), from the EU/BMBF via QuantERA (ShoQC), from the EU’s HORIZON Research and Innovation Actions (CLUSTEC), and from the Deutsche Forschungsgemeinschaft (DFG, German Research Foundation) TRR 306 QuCoLiMa (“Quantum Cooperativity of Light and Matter”).

Appendix A: Calculations

1. Representing the operators $S_\lambda(t)$ and $T_\lambda(t)$ by the polynomials P_{xx} , P_{xp} , P_{px} , and P_{pp}

Given the unitary operator \hat{U} and the set of quadratures $\mathbb{Q} = \{\hat{x}_1, \hat{p}_1, \dots, \hat{x}_n, \hat{p}_n\}$ the operator \hat{U} is well defined by its impact on the different quadratures $\hat{U}\hat{q}\hat{U}^\dagger$, $\hat{q} \in \mathbb{Q}$ up to a global phase. This can easily be seen by regarding the operator \hat{V} with $\hat{V}\hat{q}\hat{V}^\dagger = \hat{U}\hat{q}\hat{U}^\dagger$ for all $\hat{q} \in \mathbb{Q}$. Then $\hat{q} = \hat{U}^\dagger\hat{U}\hat{q}\hat{U}^\dagger\hat{U} = \hat{U}^\dagger\hat{V}\hat{q}\hat{V}^\dagger\hat{U}$ and it follows that $[\hat{q}, \hat{U}^\dagger\hat{V}] = 0$ for all $\hat{q} \in \mathbb{Q}$. Thus it must be $\hat{U}^\dagger\hat{V} = e^{i\phi} \mathbf{1}$. Calculating the impact of the operator $S_\lambda(t)$ on the four quadratures, we obtain

$$\begin{aligned} S_\lambda(t)\hat{x}_1S_\lambda(-t) &= \hat{x}_1, \\ S_\lambda(t)\hat{p}_1S_\lambda(-t) &= \hat{p}_1 - P_1[t\hat{x}_1]\hat{x}_2^2/2 - P_2[t\hat{x}_1]\hat{p}_2^2/2 - P_3[t\hat{x}_1](\hat{x}_2\hat{p}_2 + \hat{p}_2\hat{x}_2)/2, \\ S_\lambda(t)\hat{x}_2S_\lambda(-t) &= P_{xx}[t\hat{x}_1]\hat{x}_2 + P_{xp}[t\hat{x}_1]\hat{p}_2, \\ S_\lambda(t)\hat{p}_2S_\lambda(-t) &= P_{px}[t\hat{x}_1]\hat{x}_2 + P_{pp}[t\hat{x}_1]\hat{p}_2, \end{aligned} \quad (\text{A1})$$

with the polynomials P_{xx} , P_{xp} , P_{px} , P_{pp} , P_1 , P_2 , and P_3 . The former can be calculated recursively given the relations

$$\begin{aligned} P_{xx}^{(0)}[t] &= 1, & P_{xp}^{(0)}[t] &= 0, & P_{pp}^{(0)}[t] &= 1, & P_{px}^{(0)}[t] &= 0, \\ P_{xx}^{(n)}[t] &= (1 - \lambda_n\mu_n t^2) P_{xx}^{(n-1)}[t] - \lambda_n t P_{xp}^{(n-1)}[t], & P_{pp}^{(n)}[t] &= P_{pp}^{(n-1)}[t] + \mu_n t P_{px}^{(n-1)}[t], \\ P_{xp}^{(n)}[t] &= P_{xp}^{(n-1)}[t] + \mu_n t P_{xx}^{(n-1)}[t], & P_{px}^{(n)}[t] &= (1 - \lambda_n\mu_n t^2) P_{px}^{(n-1)}[t] - \lambda_n t P_{pp}^{(n-1)}[t]. \end{aligned} \quad (\text{A2})$$

On the other hand, the latter are given by

$$\begin{aligned} P_1[t] &= (\partial_t P_{xx}[t]) P_{px}[t] - P_{xx}[t] (\partial_t P_{px}[t]), \\ P_2[t] &= (\partial_t P_{xp}[t]) P_{pp}[t] - P_{xp}[t] (\partial_t P_{pp}[t]), \\ P_3[t] &= (\partial_t P_{xx}[t]) P_{pp}[t] - P_{xp}[t] (\partial_t P_{px}[t]). \end{aligned} \quad (\text{A3})$$

This can be verified by comparing the recursion formulas of both sides of the equations while using the relation

$$P_{xx}[t]P_{pp}[t] - P_{xp}[t]P_{px}[t] = 1 \quad \forall t \in \mathbb{R}. \quad (\text{A4})$$

The impact of the operator $T_\lambda(t)$ on the six quadratures is given by

$$\begin{aligned} T_\lambda(t)\hat{x}_1T_\lambda(-t) &= \hat{x}_1, & T_\lambda(t)\hat{p}_1T_\lambda(-t) &= \hat{p}_1 - P_1[t\hat{x}_1]\hat{x}_2\hat{x}_3 - P_2[t\hat{x}_1]\hat{p}_2\hat{p}_3 - P_3[t\hat{x}_1](\hat{x}_2\hat{p}_2 + \hat{p}_3\hat{x}_3), \\ T_\lambda(t)\hat{x}_2T_\lambda(-t) &= P_{xx}[t\hat{x}_1]\hat{x}_2 + P_{xp}[t\hat{x}_1]\hat{p}_3, & T_\lambda(t)\hat{p}_2T_\lambda(-t) &= P_{px}[t\hat{x}_1]\hat{x}_3 + P_{pp}[t\hat{x}_1]\hat{p}_2, \\ T_\lambda(t)\hat{x}_3T_\lambda(-t) &= P_{xx}[t\hat{x}_1]\hat{x}_3 + P_{xp}[t\hat{x}_1]\hat{p}_2, & T_\lambda(t)\hat{p}_3T_\lambda(-t) &= P_{px}[t\hat{x}_1]\hat{x}_2 + P_{pp}[t\hat{x}_1]\hat{p}_3. \end{aligned} \quad (\text{A5})$$

Therefore the operators $S_\lambda(t)$ as well as $T_\lambda(t)$ are both well defined by the four polynomials P_{xx} , P_{xp} , P_{px} , and P_{pp} . Using this alternative representation will simplify the following calculations.

2. Impact of $S_\lambda(t)$ on different input states

Here we calculate the impact of $S_\lambda(t)$ on the general two-mode input

$$|in\rangle = (\hat{S}(-\xi)|\text{vac}\rangle)_1 \left(\hat{S}(-\zeta)\hat{D}\left(\alpha/\sqrt{2}\right)|\text{vac}\rangle \right)_2, \quad (\text{A6})$$

with the squeezing operator $\hat{S}(\xi) = \exp\left(\frac{1}{2}(\xi^* \hat{a}^2 - \xi \hat{a}^{\dagger 2})\right)$ and the displacement operator $\hat{D}(\alpha) = \exp(\alpha \hat{a}^\dagger - \alpha^* \hat{a})$. Therefore we consider the two differential equations given by

$$0 = S_\lambda(t) \left(\frac{\hat{x}_1}{k_1} + ik_1 \hat{p}_1 \right) S_\lambda(-t) S_\lambda(t) |in\rangle, \quad (\text{A7})$$

$$0 = S_\lambda(t) \left(\frac{\hat{x}_2}{k_2} + ik_2 \hat{p}_2 - \alpha \right) S_\lambda(-t) S_\lambda(t) |in\rangle \quad (\text{A8})$$

when taking $\hat{p}_1 \rightarrow -i\partial_{x_1}$ and $\hat{p}_2 \rightarrow -i\partial_{x_2}$ in the position basis representation. Here, k_1 and k_2 are given by $k_1(\xi) = \left(\frac{\cosh(|\xi|) + \sinh(|\xi|) \xi/|\xi|}{\cosh(|\xi|) - \sinh(|\xi|) \xi/|\xi|} \right)^{\frac{1}{2}}$ and $k_2(\zeta) = \left(\frac{\cosh(|\zeta|) + \sinh(|\zeta|) \zeta/|\zeta|}{\cosh(|\zeta|) - \sinh(|\zeta|) \zeta/|\zeta|} \right)^{\frac{1}{2}}$. Solving Eq. (A8) using the relations of Eq. (A1), then employing Eq. (A7) and finally normalizing the result, we find that

$$\langle x_1, x_2 | S_\lambda(t) | in \rangle = \frac{e^{-\frac{\alpha^2}{2}}}{\sqrt{k_1 \pi \sqrt{B}}} \exp \left(-\frac{x_1^2}{2k_1^2} - \frac{A}{2B} x_2^2 + \frac{\alpha}{B} x_2 - \frac{\alpha^2}{2} \frac{k_2 P_{pp}[tx_1]}{B} \right), \quad (\text{A9})$$

with $A = P_{xx}[tx_1]/k_2 + ik_2 P_{px}[tx_1]$ and $B = k_2 P_{pp}[tx_1] - iP_{xp}[tx_1]/k_2$. Here the notation \sqrt{B} is used for the solution to the differential equation

$$\frac{f'(x)}{f(x)} = \frac{1}{2} \frac{B'(x)}{B(x)}. \quad (\text{A10})$$

The imaginary phase of the function $\sqrt{B}(x)$ thus covers the full range of $(-\pi, \pi]$ instead of the common $(-\frac{\pi}{2}, \frac{\pi}{2}]$. Moreover, the results are only fixed up to a global phase.

When setting $\zeta = 0$ and applying a Fourier transform in x_2 we arrive at Eq. (48) of the main text. On the other hand, setting $\xi = \alpha = 0$ and using

$$\begin{aligned} S_\lambda(t) | \text{vac} \rangle_1 (\hat{S}(-\zeta) | 1 \rangle)_2 &= S_\lambda(t) \hat{S}_2(-\zeta) \hat{a}_2^\dagger \hat{S}_2(\zeta) S_\lambda(-t) S_\lambda(t) | in \rangle = S_\lambda(t) \frac{\sqrt{2} \hat{x}_2}{k_2} S_\lambda(-t) S_\lambda(t) | in \rangle = \sqrt{2} S_\lambda(t) \\ &\times \left(\frac{\hat{x}_2}{k_2} + \frac{iP_{xp}[tx_1]}{k_2 B} \left(\frac{\hat{x}_2}{k_2} + ik_2 \hat{p}_2 \right) \right) S_\lambda(-t) S_\lambda(t) | in \rangle = \sqrt{2} \frac{\hat{x}_2}{k_2} \left(P_{xx}[tx_1] + iP_{xp}[tx_1] \frac{A}{B} \right) S_\lambda(t) | in \rangle = \frac{\sqrt{2} \hat{x}_2}{B} S_\lambda(t) | in \rangle \end{aligned} \quad (\text{A11})$$

gives us

$$\langle x_a, y | S_\lambda(t) | \text{vac} \rangle_1 (\hat{S}(-\zeta) | n_0 \rangle)_2 = \frac{\pi^{-\frac{1}{2}}}{\sqrt{B}} \left(\frac{\sqrt{2} y}{B} \right)^{n_0} \exp \left(-\frac{A}{B} \frac{y^2}{2} - \frac{x_a^2}{2} \right). \quad (\text{A12})$$

with $n_0 = 0, 1$. Applying the operator $\hat{M}^{(j)} = e^{-i\hat{x}_a/2} S_\lambda^{(a,j)}(\sqrt{\pi})$ and a Fourier transform in x_a four times to two qumode states and an ancilla

$$| \psi_{n_y, n_z} \rangle = \hat{M}^{(1)} \hat{F}_a^\dagger \hat{M}^{(2)} \hat{F}_a^\dagger \hat{M}^{(1)} \hat{F}_a^\dagger \hat{M}^{(2)} \hat{F}_a^\dagger | 0 \rangle_a | n_y \rangle | n_z \rangle, \quad (\text{A13})$$

we get

$$\begin{aligned} \psi_{n_y, n_z}(x_a, y, z) &= e^{-ix_a/2} \int \frac{dp_a}{\sqrt{2\pi}} e^{ip_a x_a + ip_a/2} \int \frac{dx'_a}{\sqrt{2\pi}} e^{-ix'_a p_a + ix'_a/2} \int \frac{dp'_a}{\sqrt{2\pi}} e^{ip'_a x'_a - ip'_a/2} \left(\frac{\sqrt{2} y}{B} \right)^{n_y} \left(\frac{\sqrt{2} z}{D} \right)^{n_z} \\ &\times \frac{\pi^{-\frac{3}{4}}}{\sqrt{BD}} \exp \left(-\frac{p_a^2}{2} - \frac{A}{B} \frac{y^2}{2} - \frac{C}{D} \frac{z^2}{2} \right), \end{aligned} \quad (\text{A14})$$

with

$$\begin{aligned} A &= P_{xx}[\sqrt{\pi} x_a] (P_{xx}[\sqrt{\pi} x'_a] - iP_{px}[\sqrt{\pi} x'_a]) + iP_{px}[\sqrt{\pi} x_a] (P_{pp}[\sqrt{\pi} x'_a] + iP_{xp}[\sqrt{\pi} x'_a]), \\ B &= P_{pp}[\sqrt{\pi} x_a] (P_{pp}[\sqrt{\pi} x'_a] + iP_{xp}[\sqrt{\pi} x'_a]) - iP_{xp}[\sqrt{\pi} x_a] (P_{xx}[\sqrt{\pi} x'_a] - iP_{px}[\sqrt{\pi} x'_a]), \\ C &= P_{xx}[\sqrt{\pi} p_a] (P_{xx}[\sqrt{\pi} p'_a] + iP_{px}[\sqrt{\pi} p'_a]) - iP_{px}[\sqrt{\pi} p_a] (P_{pp}[\sqrt{\pi} p'_a] - iP_{xp}[\sqrt{\pi} p'_a]), \\ D &= P_{pp}[\sqrt{\pi} p_a] (P_{pp}[\sqrt{\pi} p'_a] - iP_{xp}[\sqrt{\pi} p'_a]) + iP_{xp}[\sqrt{\pi} p_a] (P_{xx}[\sqrt{\pi} p'_a] + iP_{px}[\sqrt{\pi} p'_a]). \end{aligned} \quad (\text{A15})$$

The three Fourier transforms of Eq. (A14) can then be done numerically to obtain the output state of the approximate CZ gate.

3. Impact of $T_\lambda(t)$ on different input states

Next we are going to calculate the impact of $T_\lambda(t)$ on the general three-mode input

$$| in \rangle = N \int dx \int dy \int dz \phi(x) \exp \left(-\lambda \frac{y^2}{2} - \mu \frac{z^2}{2} - i\rho yz \right) | x \rangle_1 | y \rangle_2 | z \rangle_3. \quad (\text{A16})$$

As $T_\lambda(t)$ has no impact on $\phi(x)$, we can set $\phi(x) = \exp(-x^2/2)$ without loss of generality. This gives us three differential equations arising from the position space representation of

$$0 = T_\lambda(t) (\hat{x} + i\hat{p}) T_\lambda(-t) T_\lambda(t) |in\rangle, \quad (\text{A17})$$

$$0 = T_\lambda(t) (\lambda\hat{y} + i\hat{q} + i\rho\hat{z}) T_\lambda(-t) T_\lambda(t) |in\rangle, \quad (\text{A18})$$

$$0 = T_\lambda(t) (\mu\hat{z} + i\hat{r} + i\rho\hat{y}) T_\lambda(-t) T_\lambda(t) |in\rangle, \quad (\text{A19})$$

with the pairs of quadratures (\hat{x}, \hat{p}) , (\hat{y}, \hat{q}) , and (\hat{z}, \hat{r}) . The solution is given by

$$\langle x, y, z | in \rangle = \frac{N}{\sqrt{A}} \phi(x) \exp\left(-\lambda \frac{y^2}{2A} - \mu \frac{z^2}{2A} - i \frac{B}{A} yz\right), \quad (\text{A20})$$

with $A = (P_{pp}[tx] + \rho P_{xp}[tx])^2 + \lambda \mu P_{xp}^2[tx]$ and $B = (P_{pp}[tx] + \rho P_{xp}[tx]) (P_{px}[tx] + \rho P_{xx}[tx]) + \lambda \mu P_{xp}[tx] P_{xx}[tx]$. Similar to Eq. (A11) we also obtain

$$T_\lambda(t) (\alpha\hat{y} + \beta\hat{z}) |in\rangle = \left(\frac{\alpha (P_{pp}[tx] + \rho P_{xp}[tx]) + i\beta\lambda P_{xp}[tx]}{A} \hat{y} + \frac{\beta (P_{pp}[tx] + \rho P_{xp}[tx]) + i\alpha\mu P_{xp}[tx]}{A} \hat{z} \right) T_\lambda(t) |in\rangle. \quad (\text{A21})$$

When setting $u_k = 0$, one step of the protocol of Eq. (57) is given by

$$|\psi_{v_k, w_k}\rangle = \hat{F}_3 T_\lambda(w_k) \hat{F}_3^\dagger \hat{F}_1 T_\lambda(v_k) \hat{F}_1^\dagger (\alpha\hat{y} + \beta\hat{z}) |in\rangle. \quad (\text{A22})$$

Besides the two operators $T_\lambda(v_k)$ and $T_\lambda(w_k)$ the Fourier transforms in z can also be calculated analytically. Overall this leaves us with

$$\psi_{v_k, w_k}(x, y, z) = N' \int \frac{dp}{\sqrt{2\pi}} e^{ipx} \int \frac{dx'}{\sqrt{2\pi}} e^{-ix'p} (\alpha'\hat{y} + \beta'\hat{z}) \phi(x') \exp\left(-\lambda' \frac{y^2}{2} - \mu' \frac{z^2}{2} - i\rho' yz\right), \quad (\text{A23})$$

where

$$\begin{aligned} \lambda' &= \frac{\mu}{A[v_k p]} \left[\left(P_{px}[w_k x] - i \frac{B[v_k p]}{\mu} P_{xx}[w_k x] \right)^2 + \left(\frac{\lambda}{\mu} + \frac{B^2[v_k p]}{\mu^2} \right) P_{xx}^2[w_k x] \right], \\ \mu' &= \frac{\mu}{A[v_k p]} \left[\left(P_{pp}[w_k x] - i \frac{B[v_k p]}{\mu} P_{xp}[w_k x] \right)^2 + \left(\frac{\lambda}{\mu} + \frac{B^2[v_k p]}{\mu^2} \right) P_{xp}^2[w_k x] \right], \\ \rho' &= i \frac{\mu}{A[v_k p]} \left[\left(P_{pp}[w_k x] - i \frac{B[v_k p]}{\mu} P_{xp}[w_k x] \right) \left(P_{px}[w_k x] - i \frac{B[v_k p]}{\mu} P_{xx}[w_k x] \right) + \left(\frac{\lambda}{\mu} + \frac{B^2[v_k p]}{\mu^2} \right) P_{xp}[w_k x] P_{xx}[w_k x] \right], \\ \alpha' &= P_{xx}[w_k x] \frac{\alpha (P_{pp}[v_k p] + \rho P_{xp}[v_k p]) + i\beta\lambda P_{xp}[v_k p]}{A[v_k p]} - P_{px}[w_k x] \frac{\beta (P_{pp}[v_k p] + \rho P_{xp}[v_k p]) + i\alpha\mu P_{xp}[v_k p]}{A[v_k p]}, \\ \beta' &= P_{pp}[w_k x] \frac{\beta (P_{pp}[v_k p] + \rho P_{xp}[v_k p]) + i\alpha\mu P_{xp}[v_k p]}{A[v_k p]} - P_{xp}[w_k x] \frac{\alpha (P_{pp}[v_k p] + \rho P_{xp}[v_k p]) + i\beta\lambda P_{xp}[v_k p]}{A[v_k p]} \quad \text{and} \quad N' = \frac{N}{\sqrt{A[v_k p]}}. \end{aligned} \quad (\text{A24})$$

This step can be repeated for each iteration of the protocol. Calculating the Fourier transforms numerically then leaves us with the output state of the approximated measurement-free protocol.

Appendix B: Optimized parameter sets

In order to improve upon the Trotter-Suzuki decomposition the parameter sets λ are separately optimized for each application. For this the Basin-hopping algorithm implemented in Python with starting points fulfilling Eq. (31) is used. For the approximated CZ gate the worst-case fidelity defined in the main text is maximized. For the GKP states the state's fidelity towards the corresponding Gaussian GKP state is used as a figure of merit. The optimized gate sets approximating the CZ gate are

$$\begin{aligned} L = 6: & \quad [0.1917, 0.3068, 0.3478, 0.3615, 0.3199, 0.1972] \\ L = 7: & \quad [0.1453, 0.2971, 0.3045, 0.3139, 0.3057, 0.2976, 0.1485, 0] \\ L = 9: & \quad [0.1163, 0.2294, 0.2462, 0.2440, 0.2304, 0.2442, 0.2464, 0.2302, 0.1168, 0] \\ L = 11: & \quad [0.09535, 0.1918, 0.1981, 0.1946, 0.1926, 0.1985, 0.1926, 0.1946, 0.1980, 0.1920, 0.09504, 0] \\ L = 13: & \quad [0.08059, 0.1627, 0.1651, 0.1630, 0.1636, 0.1649, 0.1623, 0.1649, 0.1635, 0.1630, 0.1650, 0.1628, 0.08046, 0] \\ L = 15: & \quad [0.06972, 0.1404, 0.1418, 0.1404, 0.1413, 0.1414, 0.1403, 0.1420, 0.1402, 0.1414, 0.1412, 0.1404, 0.1418, 0.1405, 0.06964, 0] \end{aligned}$$

The optimized gate sets used for the probabilistic GKP creation scheme are

Square encoding

$$\begin{aligned} L = 3 : & \quad [0.6794, 0.4543, 0.3353, 0] \\ L = 5 : & \quad [0.5217, 0.3469, 0.2937, 0.2536, 0.1937, 0] \\ L = 7 : & \quad [0.3566, 0.2243, 0.2416, 0.2731, 0.2764, 0.2306, 0.1295, 0] \\ L = 9 : & \quad [0.02422, 0.7957, 0.4211, 0.2941, 0.2488, 0.2294, 0.2202, 0.1823, 0.08733, 0] \end{aligned}$$

Qunaught encoding

$$L = 9 : \quad [0.3433, 0.1839, 0.1593, 0.1827, 0.2088, 0.2074, 0.2037, 0.1716, 0.09903, 0]$$

Hexagonal encoding

$$L = 9 : \quad [-0.05847, -0.2111, 0.5222, 0.3127, 0.2532, 0.2260, 0.2096, 0.1735, 0.08916, 0]$$

Magic state

$$\begin{aligned} L = 16 : & \quad [0.1038, 0.07294, 0.1861, 0.1610, 0.08781, 0.09327, 0.1317, 0.1501, 0.1380, 0.1348, 0.1213, 0.1173, 0.1105, \\ & \quad 0.1096, 0.09671, 0.05178] \\ L = 21 : & \quad [0.04155, 0.08769, 0.1025, 0.05514, 0.1391, 0.1291, 0.06734, 0.07781, 0.1304, 0.1295, 0.09831, 0.07139, 0.08922, \\ & \quad 0.1150, 0.1115, 0.08428, 0.07268, 0.09360, 0.1119, 0.09423, 0.04103, 0] \\ L = 25 : & \quad [0.02913, 0.09474, 0.1146, 0.05894, 0.09529, 0.09499, 0.06886, 0.07248, 0.09725, 0.09047, 0.07591, 0.07003, 0.08284, \\ & \quad 0.08626, 0.08380, 0.07685, 0.07693, 0.07845, 0.08287, 0.08220, 0.07977, 0.07979, 0.08801, 0.07813, 0.03718, 0] \end{aligned}$$

For the deterministic GKP creation scheme the optimized gate set is

$$L = 11 : \quad [0.09506, 0.1881, 0.1951, 0.1963, 0.1907, 0.1945, 0.1919, 0.1943, 0.1972, 0.1870, 0.09451, 0]$$

The gates of the schematic circuit of Fig. 2 are given by

$$Sq = \hat{S}(-\ln(k)), \quad D_1 = \hat{D}\left(\frac{kd}{\sqrt{2}\pi}\right), \quad D_2 = \hat{D}\left(-i\frac{k^2d}{2\sqrt{2}\pi}\right), \quad X^3 = \exp(ir_j\hat{x}^3), \quad (\text{B1})$$

with $d = 2\sqrt{\pi}$ and $k = \sqrt{\frac{21}{4}}\pi$. The r_j 's are dependent on the beam splitters and can thus be adapted. Following Eq. (14) and choosing $s = \arccos\left(\frac{1}{\sqrt{3}}\right)$ leads to the weakest possible cubic phase gates with $r_1 = r_2 = 0.0643$, $r_3 = r_4 = 0.0872$, $r_5 = r_6 = 0.1304$, and $r_7 = -0.1085$. On the other hand, setting $s_1 \neq s_2 \neq s_3$ allows us to obtain $r_1 = r_2 = r_3 = r_4 = r_5 = r_6 = -r_7 = 0.1675$.

-
- [1] W. Asavanant, Y. Shiozawa, S. Yokoyama, B. Charoensombutamon, H. Emura, R. N. Alexander, S. Takeda, J. Yoshikawa, N. C. Menicucci, H. Yonezawa, and A. Furusawa, Generation of time-domain-multiplexed two-dimensional cluster state, *Science* **366**, 373 (2019).
- [2] M. V. Larsen, X. Guo, C. R. Breum, J. S. Neergaard-Nielsen, and U. L. Andersen, Deterministic generation of a two-dimensional cluster state, *Science* **366**, 369 (2019).
- [3] E. Knill, R. Laflamme, and G. J. Milburn, A scheme for efficient quantum computation with linear optics, *Nature* **409**, 46 (2001).
- [4] D. Gottesman, A. Kitaev, and J. Preskill, Encoding a qubit in an oscillator, *Phys. Rev. A* **64**, 012310 (2001).
- [5] S. D. Bartlett and W. J. Munro, Quantum teleportation of optical quantum gates, *Phys. Rev. Lett.* **90**, 117901 (2003).
- [6] K. Miyata, H. Ogawa, P. Marek, R. Filip, H. Yonezawa, J. Yoshikawa, and A. Furusawa, Implementation of a quantum cubic gate by an adaptive non-gaussian measurement, *Phys. Rev. A* **93**, 022301 (2016).
- [7] S. Konno, W. Asavanant, K. Fukui, A. Sakaguchi, F. Hanamura, P. Marek, R. Filip, J. Yoshikawa, and A. Furusawa, Non-clifford gate on optical qubits by non-linear feedforward, *Phys. Rev. Res.* **3**, 043026 (2021).
- [8] A. Sakaguchi, S. Konno, F. Hanamura, W. Asavanant, K. Takase, H. Ogawa, P. Marek, R. Filip, J.-i. Yoshikawa, E. Huntington, H. Yonezawa, and A. Furusawa, Nonlinear feedforward enabling quantum computation, *Nature Communications* **14**, 3817 (2023).
- [9] S. Lloyd and S. L. Braunstein, Quantum computation over continuous variables, *Phys. Rev. Lett.* **82**, 1784 (1999).
- [10] S. L. Braunstein and P. van Loock, Quantum information with continuous variables, *Rev. Mod. Phys.* **77**, 513 (2005).
- [11] N. C. Menicucci, P. van Loock, M. Gu, C. Weedbrook, T. C. Ralph, and M. A. Nielsen, Universal quantum computation with continuous-variable cluster states, *Phys. Rev. Lett.* **97**, 110501 (2006).
- [12] C. Weedbrook, S. Pirandola, R. García-Patrón, N. J. Cerf, T. C. Ralph, J. H. Shapiro, and S. Lloyd, Gaussian quantum information, *Rev. Mod. Phys.* **84**, 621 (2012).
- [13] N. K. Langford, S. Ramelow, R. Prevedel, W. J. Munro,

- G. J. Milburn, and A. Zeilinger, Efficient quantum computing using coherent photon conversion, *Nature* **478**, 360 (2011).
- [14] S. L. Braunstein and R. I. McLachlan, Generalized squeezing, *Phys. Rev. A* **35**, 1659 (1987).
- [15] K. Banaszek and P. L. Knight, Quantum interference in three-photon down-conversion, *Phys. Rev. A* **55**, 2368 (1997).
- [16] R. Yanagimoto, R. Nehra, R. Hamerly, E. Ng, A. Marandi, and H. Mabuchi, Quantum nondemolition measurements with optical parametric amplifiers for ultrafast universal quantum information processing, *PRX Quantum* **4**, 010333 (2023).
- [17] Note that in the terminology of nonlinear optics, the cubic and the quadratic Hamiltonians are associated with $\chi^{(3)}$ and $\chi^{(2)}$ interactions, respectively. This is the terminology used in Ref. [16], while $\chi^{(3)}$ interactions are typically much weaker than $\chi^{(2)}$ interactions. In terms of the mode operators, however, the $\chi^{(3)}$ interaction would be of 4th order like the well-known Kerr interactions and the “quadratic” $\chi^{(2)}$ interaction would correspond to a cubic Hamiltonian. The latter is the terminology of the present work. In a way, the “cubic gates” as used here thus belong to the class of quadratic nonlinear interactions when the above terminology is applied. Nonetheless, we shall stick to the usual terminology of CV quantum computation [9–12] where the cubic gates represent the lowest-order nonlinear, non-Gaussian operations. Quadratic gates then correspond to the Gaussian gates and quadratic Hamiltonians generate the Gaussian (unitary) transformations.
- [18] M. J. Bremner, A. Montanaro, and D. J. Shepherd, Average-case complexity versus approximate simulation of commuting quantum computations, *Phys. Rev. Lett.* **117**, 080501 (2016).
- [19] T. Douce, D. Markham, E. Kashefi, E. Diamanti, T. Coudreau, P. Milman, P. van Loock, and G. Ferrini, Continuous-variable instantaneous quantum computing is hard to sample, *Phys. Rev. Lett.* **118**, 070503 (2017).
- [20] J. Hastrup, K. Park, J. B. Brask, R. Filip, and U. L. Andersen, Universal unitary transfer of continuous-variable quantum states into a few qubits, *Phys. Rev. Lett.* **128**, 110503 (2022).
- [21] C. W. S. Chang, C. Sabín, P. Forn-Díaz, F. Quijandría, A. M. Vadiraj, I. Nsanzineza, G. Johansson, and C. M. Wilson, Observation of three-photon spontaneous parametric down-conversion in a superconducting parametric cavity, *Phys. Rev. X* **10**, 011011 (2020).
- [22] Y. Zheng, O. Hahn, P. Stadler, P. Holmvall, F. Quijandría, A. Ferraro, and G. Ferrini, Gaussian conversion protocols for cubic phase state generation, *PRX Quantum* **2**, 010327 (2021).
- [23] N. Imoto, H. A. Haus, and Y. Yamamoto, Quantum nondemolition measurement of the photon number via the optical kerr effect, *Phys. Rev. A* **32**, 2287 (1985).
- [24] P. D. Drummond, J. Breslin, and R. M. Shelby, Quantum-nondemolition measurements with coherent soliton probes, *Phys. Rev. Lett.* **73**, 2837 (1994).
- [25] M. Gu, C. Weedbrook, N. C. Menicucci, T. C. Ralph, and P. van Loock, Quantum computing with continuous-variable clusters, *Phys. Rev. A* **79**, 062318 (2009).
- [26] A. P. Lund, A. Laing, S. Rahimi-Keshari, T. Rudolph, J. L. O’Brien, and T. C. Ralph, Boson sampling from a gaussian state, *Phys. Rev. Lett.* **113**, 100502 (2014).
- [27] C. S. Hamilton, R. Kruse, L. Sansoni, S. Barkhofen, C. Silberhorn, and I. Jex, Gaussian boson sampling, *Phys. Rev. Lett.* **119**, 170501 (2017).
- [28] K. K. Sabapathy, H. Qi, J. Izaac, and C. Weedbrook, Production of photonic universal quantum gates enhanced by machine learning, *Phys. Rev. A* **100**, 012326 (2019).
- [29] I. Tzitrin, J. E. Bourassa, N. C. Menicucci, and K. K. Sabapathy, Progress towards practical qubit computation using approximate Gottesman-Kitaev-Preskill codes, *Phys. Rev. A* **101**, 032315 (2020).
- [30] M. Eaton, C. González-Arciniegas, R. N. Alexander, N. C. Menicucci, and O. Pfister, Measurement-based generation and preservation of cat and grid states within a continuous-variable cluster state, *Quantum* **6**, 769 (2022).
- [31] K. Fukui, S. Takeda, M. Endo, W. Asavanant, J. Yoshikawa, P. van Loock, and A. Furusawa, Efficient backcasting search for optical quantum state synthesis, *Phys. Rev. Lett.* **128**, 240503 (2022).
- [32] J. Hastrup, M. V. Larsen, J. S. Neergaard-Nielsen, N. C. Menicucci, and U. L. Andersen, Unsuitability of cubic phase gates for non-clifford operations on Gottesman-Kitaev-Preskill states, *Phys. Rev. A* **103**, 032409 (2021).
- [33] B. Royer, S. Singh, and S. Girvin, Encoding qubits in multimode grid states, *PRX Quantum* **3**, 010335 (2022).
- [34] M. A. Nielsen and I. L. Chuang, *Quantum Computation and Quantum Information: 10th Anniversary Edition* (Cambridge University Press, 2010).
- [35] R. Raussendorf and H. J. Briegel, A one-way quantum computer, *Phys. Rev. Lett.* **86**, 5188 (2001).
- [36] Explicitly, this can be seen as follows: $e^{it^2\hat{x}^2} = e^{-i\frac{t^4}{27}} e^{i\frac{t}{3}\hat{p}} e^{it\hat{x}^3} e^{-i\frac{t}{3}\hat{p}} e^{-it\hat{x}^3} e^{-i\frac{t^2}{3}\hat{x}}$, using the momentum-operator Heisenberg transformation $e^{-it\hat{x}^3}\hat{p}e^{it\hat{x}^3} = \hat{p} + 3t\hat{x}^2$, as introduced in Sec. II E, and one of the well-known Baker-Campbell-Hausdorff (BCH) formulas.
- [37] A. Furusawa and P. van Loock, *Quantum Teleportation and Entanglement* (John Wiley & Sons, Ltd, 2011).
- [38] S. Sefi and P. van Loock, How to decompose arbitrary continuous-variable quantum operations, *Phys. Rev. Lett.* **107**, 170501 (2011).
- [39] S. D. Bartlett, B. C. Sanders, S. L. Braunstein, and K. Nemoto, Efficient classical simulation of continuous variable quantum information processes, *Phys. Rev. Lett.* **88**, 097904 (2002).
- [40] J. Niset, J. Fiurášek, and N. J. Cerf, No-go theorem for gaussian quantum error correction, *Phys. Rev. Lett.* **102**, 120501 (2009).
- [41] R. Namiki, O. Gittsovich, S. Guha, and N. Lütkenhaus, Gaussian-only regenerative stations cannot act as quantum repeaters, *Phys. Rev. A* **90**, 062316 (2014).
- [42] F. Schmidt and P. van Loock, Quantum error correction with higher Gottesman-Kitaev-Preskill codes: Minimal measurements and linear optics, *Phys. Rev. A* **105**, 042427 (2022).
- [43] J. Conrad, J. Eisert, and F. Arzani, Gottesman-Kitaev-Preskill codes: A lattice perspective, *Quantum* **6**, 648 (2022).
- [44] L. Hänggli, M. Heinze, and R. König, Enhanced noise resilience of the surface-Gottesman-Kitaev-Preskill code via designed bias, *Phys. Rev. A* **102**, 052408 (2020).

- [45] K. Noh and C. Chamberland, Fault-tolerant bosonic quantum error correction with the surface-gottesman-kitaev-preskill code, *Phys. Rev. A* **101**, 012316 (2020).
- [46] C. Vuillot, H. Asasi, Y. Wang, L. P. Pryadko, and B. M. Terhal, Quantum error correction with the toric gottesman-kitaev-preskill code, *Phys. Rev. A* **99**, 032344 (2019).
- [47] K. Fukui, A. Tomita, A. Okamoto, and K. Fujii, High-threshold fault-tolerant quantum computation with analog quantum error correction, *Phys. Rev. X* **8**, 021054 (2018).
- [48] K. Fukui, A. Tomita, and A. Okamoto, Analog quantum error correction with encoding a qubit into an oscillator, *Phys. Rev. Lett.* **119**, 180507 (2017).
- [49] A. L. Grimsmo, J. Combes, and B. Q. Baragiola, Quantum computing with rotation-symmetric bosonic codes, *Phys. Rev. X* **10**, 011058 (2020).
- [50] M. H. Michael, M. Silveri, R. T. Brierley, V. V. Albert, J. Salmilehto, L. Jiang, and S. M. Girvin, New class of quantum error-correcting codes for a bosonic mode, *Phys. Rev. X* **6**, 031006 (2016).
- [51] M. Bergmann and P. van Loock, Quantum error correction against photon loss using multicomponent cat states, *Phys. Rev. A* **94**, 042332 (2016).
- [52] M. Bergmann and P. van Loock, Quantum error correction against photon loss using noon states, *Phys. Rev. A* **94**, 012311 (2016).
- [53] Z. Leghtas, G. Kirchmair, B. Vlastakis, R. J. Schoelkopf, M. H. Devoret, and M. Mirrahimi, Hardware-efficient autonomous quantum memory protection, *Phys. Rev. Lett.* **111**, 120501 (2013).
- [54] I. L. Chuang, D. W. Leung, and Y. Yamamoto, Bosonic quantum codes for amplitude damping, *Phys. Rev. A* **56**, 1114 (1997).
- [55] A. L. Grimsmo and S. Puri, Quantum error correction with the gottesman-kitaev-preskill code, *PRX Quantum* **2**, 020101 (2021).
- [56] H. Yamasaki, T. Matsuura, and M. Koashi, Cost-reduced all-gaussian universality with the gottesman-kitaev-preskill code: Resource-theoretic approach to cost analysis, *Phys. Rev. Res.* **2**, 023270 (2020).
- [57] B. Q. Baragiola, G. Pantaleoni, R. N. Alexander, A. Karanjai, and N. C. Menicucci, All-gaussian universality and fault tolerance with the gottesman-kitaev-preskill code, *Phys. Rev. Lett.* **123**, 200502 (2019).
- [58] F. Ewert and P. van Loock, Teleportation-assisted optical controlled-sign gates, *Phys. Rev. A* **99**, 032333 (2019).
- [59] M. A. Nielsen, Optical quantum computation using cluster states, *Phys. Rev. Lett.* **93**, 040503 (2004).
- [60] D. E. Browne and T. Rudolph, Resource-efficient linear optical quantum computation, *Phys. Rev. Lett.* **95**, 010501 (2005).
- [61] M. Varnava, D. E. Browne, and T. Rudolph, Loss tolerance in one-way quantum computation via counterfactual error correction, *Phys. Rev. Lett.* **97**, 120501 (2006).
- [62] S. L. Braunstein, Squeezing as an irreducible resource, *Phys. Rev. A* **71**, 055801 (2005).
- [63] T. Yamazaki, T. Arizono, T. Kobayashi, R. Ikuta, and T. Yamamoto, Linear optical quantum computation with frequency-comb qubits and passive devices, *Phys. Rev. Lett.* **130**, 200602 (2023).
- [64] N. Fabre, G. Maltese, F. Appas, S. Felicetti, A. Ketterer, A. Keller, T. Coudreau, F. Baboux, M. I. Amanti, S. Ducci, and P. Milman, Generation of a time-frequency grid state with integrated biphoton frequency combs, *Phys. Rev. A* **102**, 012607 (2020).
- [65] M. Suzuki, Fractal decomposition of exponential operators with applications to many-body theories and monte carlo simulations, *Phys. Lett. A* **146**, 319 (1990).
- [66] M. Suzuki, General theory of fractal path integrals with applications to many-body theories and statistical physics, *J. Math. Phys.* **32**, 400 (1991).
- [67] The possibility and usefulness of an exact decomposition for some given nonlinear gates were first pointed out in Refs. [38, 70]. A more systematic treatment, exploring more generally which gate classes may be exactly decomposed, was presented later in Ref. [68].
- [68] T. Kalajdziewski and J. M. Arrazola, Exact gate decompositions for photonic quantum computing, *Phys. Rev. A* **99**, 022341 (2019).
- [69] R. Ukai, J. Yoshikawa, N. Iwata, P. van Loock, and A. Furusawa, Universal linear bogoliubov transformations through one-way quantum computation, *Phys. Rev. A* **81**, 032315 (2010).
- [70] S. Sefi, V. Vaibhav, and P. van Loock, Measurement-induced optical kerr interaction, *Phys. Rev. A* **88**, 012303 (2013).
- [71] Here we use the convention $\hbar = 1$ throughout. Generally, one has $e^{-ir\hat{x}^3} \hat{p} e^{ir\hat{x}^3} = \hat{p} + [\hat{p}, ir\hat{x}^3] = \hat{p} + 3\hbar r\hat{x}^2$ using the BCH formula $e^{-B} A e^B = A + [A, B]$ (where the additional nested commutators of the sum have vanished) with $[\hat{x}^3, \hat{p}] = 3i\hbar\hat{x}^2$.
- [72] M. Yukawa, K. Miyata, H. Yonezawa, P. Marek, R. Filip, and A. Furusawa, Emulating quantum cubic nonlinearity, *Phys. Rev. A* **88**, 053816 (2013).
- [73] S. Konno, A. Sakaguchi, W. Asavanant, H. Ogawa, M. Kobayashi, P. Marek, R. Filip, J. Yoshikawa, and A. Furusawa, Nonlinear squeezing for measurement-based non-gaussian operations in time domain, *Phys. Rev. Appl.* **15**, 024024 (2021).
- [74] B. D. M. Jones, D. R. White, G. O. O'Brien, J. A. Clark, and E. T. Campbell, Optimising trotter-suzuki decompositions for quantum simulation using evolutionary strategies, in *Proceedings of the Genetic and Evolutionary Computation Conference, GECCO '19* (Association for Computing Machinery, New York, NY, USA, 2019) p. 1223–1231.
- [75] This is unlike previous treatments that rely upon non-optical platforms with more natural Rabi-type interactions [107] or similarly on dispersive atom-light interactions in cavityQED [108], or, alternatively, in a certain instance of an optical two-mode Rabi-type interaction including an optical “single-mode qubit”, on probabilistic conditional operations [109]. Our scheme, of course, would still fundamentally depend on the availability of optical single-mode cubic phase gates. In some of the other treatments, the initial setting is somewhat converse compared with ours: Rabi-type qumode-qubit interactions including a physical two-level qubit system are assumed to be available and then concatenated to obtain, for instance, a qumode (e.g., optical) single-mode cubic (or even higher) phase gate [110].
- [76] J. L. O'Brien, G. J. Pryde, A. G. White, T. C. Ralph, and D. Branning, Demonstration of an all-optical quantum controlled-not gate, *Nature* **426**, 264 (2003).

- [77] N. Kiesel, C. Schmid, U. Weber, R. Ursin, and H. Weinfurter, Linear optics controlled-phase gate made simple, *Phys. Rev. Lett.* **95**, 210505 (2005).
- [78] R. Okamoto, H. F. Hofmann, S. Takeuchi, and K. Sasaki, Demonstration of an optical quantum controlled-not gate without path interference, *Phys. Rev. Lett.* **95**, 210506 (2005).
- [79] N. K. Langford, T. J. Weinhold, R. Prevedel, K. J. Resch, A. Gilchrist, J. L. O'Brien, G. J. Pryde, and A. G. White, Demonstration of a simple entangling optical gate and its use in bell-state analysis, *Phys. Rev. Lett.* **95**, 210504 (2005).
- [80] S. Gasparoni, J.-W. Pan, P. Walther, T. Rudolph, and A. Zeilinger, Realization of a photonic controlled-not gate sufficient for quantum computation, *Phys. Rev. Lett.* **93**, 020504 (2004).
- [81] Z. Zhao, A.-N. Zhang, Y.-A. Chen, H. Zhang, J.-F. Du, T. Yang, and J.-W. Pan, Experimental demonstration of a nondestructive controlled-not quantum gate for two independent photon qubits, *Phys. Rev. Lett.* **94**, 030501 (2005).
- [82] Y.-F. Huang, X.-F. Ren, Y.-S. Zhang, L.-M. Duan, and G.-C. Guo, Experimental teleportation of a quantum controlled-not gate, *Phys. Rev. Lett.* **93**, 240501 (2004).
- [83] J. Zeuner, A. N. Sharma, M. Tillmann, R. Heilmann, M. Gräfe, A. Moqanaki, A. Szameit, and P. Walther, Integrated-optics heralded controlled-not gate for polarization-encoded qubits, *npj Quantum Inf.* **4**, 13 (2018).
- [84] K. Nemoto and W. J. Munro, Nearly deterministic linear optical controlled-not gate, *Phys. Rev. Lett.* **93**, 250502 (2004).
- [85] J. H. Shapiro, Single-photon kerr nonlinearities do not help quantum computation, *Phys. Rev. A* **73**, 062305 (2006).
- [86] T. Douce, D. Markham, E. Kashefi, P. van Loock, and G. Ferrini, Probabilistic fault-tolerant universal quantum computation and sampling problems in continuous variables, *Phys. Rev. A* **99**, 012344 (2019).
- [87] M. T. Johnsson, P. M. Poggi, M. A. Rodriguez, R. N. Alexander, and J. Twamley, Generating nonlinearities from conditional linear operations, squeezing, and measurement for quantum computation and superheisenberg sensing, *Phys. Rev. Res.* **3**, 023222 (2021).
- [88] P. Campagne-Ibarcq, A. Eickbusch, S. Touzard, E. Zalys-Geller, N. Frattini, V. Sivak, P. Reinhold, S. Puri, S. Shankar, R. Schoelkopf, L. Frunzio, M. Mirrahimi, and M. Devoret, Quantum error correction of a qubit encoded in grid states of an oscillator, *Nature* **584**, 368 (2020).
- [89] C. Flühmann, T. Nguyen, M. Marinelli, V. Negnevitsky, K. Mehta, and J. Home, Encoding a qubit in a trapped-ion mechanical oscillator, *Nature* **566**, 513 (2019).
- [90] S. Konno, W. Asavanant, F. Hanamura, H. Nagayoshi, K. Fukui, A. Sakaguchi, R. Ide, F. China, M. Yabuno, S. Miki, H. Terai, K. Takase, M. Endo, P. Marek, R. Filip, P. van Loock, and A. Furusawa, Logical states for fault-tolerant quantum computation with propagating light, *Science* **383**, 289 (2024).
- [91] N. Quesada, L. G. Helt, J. Izaac, J. M. Arrazola, R. Shahrokhshahi, C. R. Myers, and K. K. Sabapathy, Simulating realistic non-gaussian state preparation, *Phys. Rev. A* **100**, 022341 (2019).
- [92] D. Su, C. R. Myers, and K. K. Sabapathy, Conversion of gaussian states to non-gaussian states using photon-number-resolving detectors, *Phys. Rev. A* **100**, 052301 (2019).
- [93] H. M. Vasconcelos, L. Sanz, and S. Glancy, All-optical generation of states for “encoding a qubit in an oscillator”, *Opt. Lett.* **35**, 3261 (2010).
- [94] S. Pirandola, S. Mancini, D. Vitali, and P. Tombesi, Constructing finite-dimensional codes with optical continuous variables, *EPL* **68**, 323 (2004).
- [95] K. Fukui, M. Endo, W. Asavanant, A. Sakaguchi, J. Yoshikawa, and A. Furusawa, Generating the Gottesman-Kitaev-Preskill qubit using a cross-kerr interaction between squeezed light and Fock states in optics, *Phys. Rev. A* **105**, 022436 (2022).
- [96] J. Hastrup, K. Park, J. B. Brask, R. Filip, and U. L. Andersen, Measurement-free preparation of grid states, *npj Quantum Inf.* **7**, 17 (2021).
- [97] B. W. Walshe, B. Q. Baragiola, R. N. Alexander, and N. C. Menicucci, Continuous-variable gate teleportation and bosonic-code error correction, *Phys. Rev. A* **102**, 062411 (2020).
- [98] T. Matsuura, H. Yamasaki, and M. Koashi, Equivalence of approximate Gottesman-Kitaev-Preskill codes, *Phys. Rev. A* **102**, 032408 (2020).
- [99] V. V. Albert, K. Noh, K. Duivenvoorden, D. J. Young, R. T. Brierley, P. Reinhold, C. Vuillot, L. Li, C. Shen, S. M. Girvin, B. M. Terhal, and L. Jiang, Performance and structure of single-mode bosonic codes, *Phys. Rev. A* **97**, 032346 (2018).
- [100] However, note that there is a very recent quantum optical experiment demonstrating the creation of photonic states with GKP-type features [90].
- [101] D. J. Weigand and B. M. Terhal, Realizing modular quadrature measurements via a tunable photon-pressure coupling in circuit qed, *Phys. Rev. A* **101**, 053840 (2020).
- [102] B. de Neeve, T.-L. Nguyen, T. Behrle, and J. P. Home, Error correction of a logical grid state qubit by dissipative pumping, *Nat. Phys.* **18**, 296 (2022).
- [103] A. Eickbusch, V. Sivak, A. Z. Ding, S. S. Elder, S. R. Jha, J. Venkatraman, B. Royer, S. M. Girvin, R. J. Schoelkopf, and M. H. Devoret, Fast universal control of an oscillator with weak dispersive coupling to a qubit, *Nat. Phys.* **18**, 1464 (2022).
- [104] N. C. Menicucci, Fault-tolerant measurement-based quantum computing with continuous-variable cluster states, *Phys. Rev. Lett.* **112**, 120504 (2014).
- [105] J. Yoshikawa, K. Makino, S. Kurata, P. van Loock, and A. Furusawa, Creation, storage, and on-demand release of optical quantum states with a negative Wigner function, *Phys. Rev. X* **3**, 041028 (2013).
- [106] Y. Hashimoto, T. Toyama, J. Yoshikawa, K. Makino, F. Okamoto, R. Sakakibara, S. Takeda, P. van Loock, and A. Furusawa, All-optical storage of phase-sensitive quantum states of light, *Phys. Rev. Lett.* **123**, 113603 (2019).
- [107] K. Park, P. Marek, and R. Filip, Qubit-mediated deterministic nonlinear gates for quantum oscillators, *Sci. Rep.* **7**, 11536 (2017).
- [108] P. van Loock, W. J. Munro, K. Nemoto, T. P. Spiller, T. D. Ladd, S. L. Braunstein, and G. J. Milburn, Hybrid quantum computation in quantum optics, *Phys. Rev. A* **78**, 022303 (2008).
- [109] K. Park, J. Laurat, and R. Filip, Hybrid Rabi interac-

tions with traveling states of light, *New J. Phys.* **22**, 013056 (2020).

[110] K. Park, P. Marek, and R. Filip, Deterministic nonlinear

phase gates induced by a single qubit, *New J. Phys.* **20**, 053022 (2018).